Geochemistry Geophysics Geosystems G3
AN ELECTRONIC JOURNAL OF THE EARTH SCIENCES
Published by AGU and the Geochemical Society

Article
Volume 9, Number 9
18 September 2008
Q09001, doi:10.1029/2008GC002057
ISSN: 1525-2027

Petrology of some oceanic island basalts: PRIMELT2.XLS software for primary magma calculation

C. Herzberg
Earth and Planetary Sciences, Rutgers University, Piscataway, New Jersey 08854, USA (herzberg@rci.rutgers.edu)

P. D. Asimow
Geological and Planetary Sciences, California Institute of Technology, Pasadena, California 91125, USA

[1] PRIMELT2.XLS software is introduced for calculating primary magma composition and mantle potential temperature (T_P) from an observed lava composition. It is an upgrade over a previous version in that it includes garnet peridotite melting and it detects complexities that can lead to overestimates in T_P by >100°C. These are variations in source lithology, source volatile content, source oxidation state, and clinopyroxene fractionation. Nevertheless, application of PRIMELT2.XLS to lavas from a wide range of oceanic islands reveals no evidence that volatile-enrichment and source fertility are sufficient to produce them. All are associated with thermal anomalies, and this appears to be a prerequisite for their formation. For the ocean islands considered in this work, T_P maxima are typically ~1450–1500°C in the Atlantic and 1500–1600°C in the Pacific, substantially greater than ~1350°C for ambient mantle. Lavas from the Galápagos Islands and Hawaii record in their geochemistry high T_P maxima and large ranges in both T_P and melt fraction over short horizontal distances, a result that is predicted by the mantle plume model.

Components: 14,488 words, 12 figures, 1 table.

Keywords: mantle plumes; oceanic island basalts; mantle potential temperature; primary magma.

Index Terms: 3621 Mineralogy and Petrology: Mantle processes (1038); 3610 Mineralogy and Petrology: Geochemical modeling (1009, 8410); 3630 Mineralogy and Petrology: Experimental mineralogy and petrology.

Received 10 April 2008; **Revised** 2 July 2008; **Accepted** 15 July 2008; **Published** 18 September 2008.

Herzberg, C., and P. D. Asimow (2008), Petrology of some oceanic island basalts: PRIMELT2.XLS software for primary magma calculation, *Geochem. Geophys. Geosyst.*, *9*, Q09001, doi:10.1029/2008GC002057.

1. Introduction

[2] The temperature of ambient mantle and the existence of possible thermal anomalies are fundamental properties of the Earth. Because temperature always increases with depth, a comparison of temperature variations is commonly made using a 1 atmosphere reference frame termed the mantle potential temperature T_P [*McKenzie and Bickle*, 1988]. This is the temperature that the solid adiabatically convecting mantle would attain if it could reach the surface without melting. Magmas record these T_P variations in their petrology and major element geochemistry. This is known because simulations of mantle melting in controlled laboratory experiments reveal that dry hot mantle peridotite will produce magmas with higher MgO contents than mantle that is cooler. The problem is how exactly mantle temperature can be inferred from the geochemistry of an erupted lava.

[3] In principle, a calibration and parameterization of laboratory data can be applied to mafic-ultramafic volcanic rocks, and the thermal state of their source can be inferred. There are, however, processes that occur in nature that complicate a direct comparison of laboratory and field observations. Magma generation in the mantle occurs by fractional melting, and this produces primary magmas that cannot be easily simulated in the laboratory [*Asimow and Longhi*, 2004]. Moreover, fractional crystallization in both the crust and mantle can change the geochemistry of primary magmas. It is important to understand the details of the partial melting and crystallization processes because they can greatly impact inferences about mantle source temperature [*Herzberg et al.*, 2007].

[4] It is rarely practical for any one geologist to infer the temperature of the mantle that melts below a volcano by an integrated field, laboratory, and theoretical study. Consequently, we have provided petrological software, called PRIMELT1, that synthesizes much of the laboratory and theoretical component with the goal that it should be simple and accurate to use [*Herzberg et al.*, 2007]. PRIMELT software uses a mass balance solution to the primary magma problem calibrated to fertile peridotite KR-4003, derived from a parameterization [*Herzberg and O'Hara*, 2002; *Herzberg*, 2004, 2006] of experimentally determined partial melt compositions [*Walter*, 1998], and incorporates corrections for limited ranges of source heterogeneity. It uniquely constrains the primary magma composition corresponding to a given evolved lava by computing a melt fraction that is common to both partial melts of mantle peridotite and to the primitive magmas from which the lava was derived. In this way, it differs from other methods that use olivine composition to constrain primary magma composition [e.g., *Putirka*, 2005; *Courtier et al.*, 2007].

[5] PRIMELT2 models primary magma compositions that form by accumulated perfect fractional melting. Fractional melting has been calculated as a series of small increments of equilibrium melting followed by extraction of all of the melt [*Herzberg and O'Hara*, 2002]. Results for major elements are not significantly affected by including a small trapped melt fraction within a residual porosity. Melting begins at a specified pressure, the instantaneous parcel of melt is in equilibrium with its residue, and it is subsequently removed. The residue changes in composition owing to this melt removal, and it moves upward where it melts to yield another instantaneous parcel of liquid, a process that is repeated many times until melting terminates at some lower pressure. It is assumed that the instantaneous parcels of melt mix with one another, and the composition of the "pooled" or "aggregated" melt is the average composition of all the melt fractions [*Shaw*, 1970]. It is the accumulated fractional melt that is identified as the primary magma. Its composition is calculated by PRIMELT1 software, as originally described by *Herzberg and O'Hara* [2002] and illustrated as a tutorial in the appendix of *Herzberg et al.* [2007]. The tutorial guides the reader through the details of the method by providing a step-by-step example of how melt fraction can be used to solve a primary magma composition. An abbreviated refresher on methodology is given again in section 2, but the details of this tutorial will not be repeated.

[6] There were important limitations to PRIMELT1 that were discussed [*Herzberg et al.*, 2007]. The resolution to some of these limitations is provided by its successor, PRIMELT2, given in the present paper. One problem is that PRIMELT1 is only successful for magmas that separated from residues of spinel lherzolite, lherzolite, harzburgite, and dunite; it is not suitable for garnet peridotite residues. For many oceanic islands, whose melting regions lie at relatively high pressure, PRIMELT1 consequently calculates MgO contents that are about 2 weight % too high, propagating to a potential temperature that is too high by about 50°C. This limitation has been corrected with PRIMELT2.

[7] PRIMELT1 was not equipped to evaluate uncertainties that arise from variations in source lithology, source volatile content, or source oxidation state. Uncertainties arising from clinopyroxene fractionation in the crust were discussed [*Herzberg et al.*, 2007], but this can also occur in the mantle [*Irving*, 1980; *Frey*, 1980; *Sen*, 1988; *Albarède et al.*, 1997; *Keshav et al.*, 2007]. These shortcomings are explicitly considered in this paper, and their effects are evaluated with PRIMELT2.

[8] In this work we summarize the improvements that make PRIMELT2 suitable for use in modeling oceanic island basalts. The changes are described by application of PRIMELT2 to lava compositions from oceanic island basalts from the Azores, Canaries, Cook-Austral, Galápagos, Hawaii, Iceland, Marquesas, Pitcairn-Gambier, St. Helena, Samoa, Society, and Tristan da Cunha. Lava analyses were obtained from GEOROC (http://georoc.mpch-mainz.gwdg.de/georoc/). Original samples and the primary

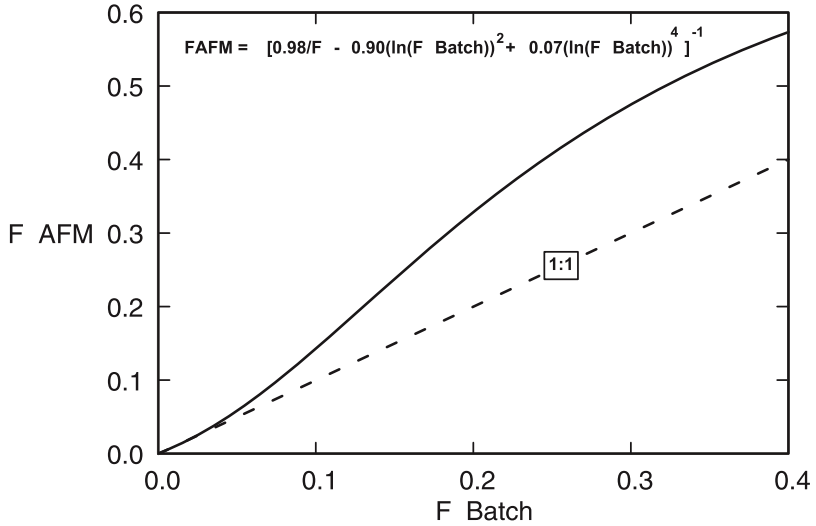

Figure 1. The relationship between melt fraction for batch melting, F Batch, and accumulated fractional melting, F AFM, for a magma with a specific content of MgO and FeO.

sources that provided successful primary magma solutions are identified in Appendix A1.

[9] Some notes are provided in Appendix A2 on the use of the PRIMELT2.XLS implementation (which is provided as auxiliary material Software S1[1]). The calculations permit inferences to be made about mantle potential temperature and melt fraction. They also expedite an evaluation of petrological contributions to error in computed mantle potential temperature. The results have new implications for the mantle plume model.

2. Melt Fractions

[10] A lava composition is selected for which olivine is thought to have been the only crystallizing phase; the selection is sometimes straightforward and based on a variety of diagrams that examine the liquid line of descent for rock compositions with more than about 8% MgO [*Herzberg et al.*, 2007]. To this lava composition, olivine is added or subtracted in a series of small increments, yielding an array of potential primary magma compositions. For each liquid composition along this olivine-control array, the melt fraction F is computed for the case of batch melting by rearranging equations (22) and (23) of *Herzberg and O'Hara* [2002] to

$$F = (D_{FeO}MgO_L - 38.12K_D)/(D_{FeO}MgO_L - K_DMgO_L) \quad (1)$$

where K_D is the FeO-MgO exchange coefficient at pressures within the melting regime [*Herzberg and O'Hara*, 2002]:

$$K_D = 0.3813 - 0.7896/MgO_L + 1.0389/(MgO_L)^2 \quad (2)$$

Equation (2) yields values for K_D that are in good agreement with the parameterization of *Toplis* [2005]. MgO_L is the weight % MgO content of the liquid, and 38.12 is the weight % MgO content of fertile peridotite KR-4003 source. D_{FeO} is the bulk distribution coefficient for FeO, which is the weight % of peridotite KR-4003 (i.e., 8.02%) divided by the weight % FeO of the liquid; the latter quantity is obtained by the addition/subtraction of olivine from a lava composition.

[11] For any primary magma with a specific content of MgO and FeO, the amount of melting needed to produce it for the case of accumulated fractional melting is always greater than or equal to that for batch melting [*Herzberg and O'Hara*, 2002]. From that work, the melt fraction for accumulated fractional melting, FAFM, can be derived from the melt fraction for batch melting, F, using the following relation:

$$FAFM = \left[0.98/F - 0.90(\ln(F))^2 + 0.07(\ln(F))^4\right]^{-1} \quad (3)$$

Results are shown in Figure 1. One consequence of this relationship is that the melt fraction FAFM is uniquely defined by the MgO and FeO contents of any accumulated fractional melt. It does not depend on the temperatures and pressures at which melting begins and ends, and applies to all polybaric and isobaric

Auxiliary materials are available in the HTML. doi:10.1029/2008GC002057.

accumulated fractional melting paths [*Herzberg and O'Hara*, 2002, p. 1869], a result that is not intuitively obvious. But in nature mantle peridotite melts progressively during decompression along an adiabatic T-P path, generating accumulated fractional melts with lower FeO at nearly constant MgO [*Herzberg and O'Hara*, 2002]. Examples are discussed below.

[12] In the hybrid forward-inverse method of *Herzberg and O'Hara* [2002], the melt fractions derived by olivine addition or subtraction from observed lava compositions are compared to melt fractions calculated from parameterizations of melting experiments. The results of melting experiments are recomputed in CIPW norm-like components of Olivine-Anorthite-Diopside-Silica. Melt fraction expressions are developed by examining the compositions in projection and contouring these projected results. Here we use three expressions that capture the behavior of melt fraction in projection for three different residual lithologies (Figure A1d) [*Herzberg and O'Hara*, 2002]:

$$F1 = 6.2819An^2 - 14.7789An^3 + 0.00825(1/An)^2 \quad (4)$$

for melt extraction from residues of harzburgite and dunite,

$$F2 = -2.3584 + 1.7643^*(An + 0.294Ol) + 0.7881/(An + 0.294Ol) \quad (5)$$

for melt extraction from residues of spinel lherzolite and lherzolite, and

$$F3 = 6.3471 - 10.081/(An + 0.705Ol) + 4.0022/(An + 0.705Ol)^2 \quad (6)$$

for residues of garnet peridotite. An and Ol in equations (4) to (6) are projection coordinates for liquids that project from diopside into the plane olivine-anorthite-silica (see caption to Figure 2 of *Herzberg et al.* [2007]).

[13] Melt fractions derived from equations (1) to (6) are used by PRIMELT2 to compute primary magma composition. As discussed above and by *Herzberg et al.* [2007], olivine is first added and/or subtracted from a representative lava composition. This produces an array of possible primary magma compositions from which PRIMELT2 calculates melt fraction from FeO and MgO using equation (3). From this same array, melt fractions F1-F3 in projection space are calculated using equations (4) to (6). Of all the potential primary magmas along this array, there can only be one having the same melt fraction in both FeO-MgO and projection space [*Herzberg and O'Hara*, 2002; *Herzberg et al.*, 2007]. This is the model primary magma composition. It is calculated by PRIMELT2 when there is equality of melt fraction in FeO-MgO and projection space. We note that regions in projection space filled by melts from the three different lithologies are non-overlapping and PRIMELT2 can automatically select whether F1, F2, or F3 is the relevant quantity to compare to F or FAFM from equations (1) and (3). Although the problem is constrained using FeO-MgO and projection space, the solution must be internally consistent for all major elements as discussed in Appendix A3. This is a mass balance solution to the primary magma problem, given the assumption that the initial source composition is fertile peridotite. Solutions for MgO permit inferences to be made about mantle potential temperature (section 10).

[14] The MgO content of calculated primary magmas are not strongly affected by several important uncertainties in the phase equilibrium properties of garnet peridotite melting. One is uncertainty in F3 owing to the very limited number of experiments on low-degree melts of any garnet peridotite. Another is a great deal of variability to pyroxene-garnet phase relations that can arise from small changes in fertile peridotite composition [*Herzberg and Zhang*, 1996; *Longhi and Bertka*, 1996; *Longhi*, 2002]. As shown in section 9, melt fractions that vary from 0 to 0.10, a large range owing possibly to the above uncertainties, yield primary magmas with MgO contents that differ by $\sim$1.0–1.5%, obtained from FeO-MgO-FAFM systematics in equations (1) to (3). This range in MgO would propagate to an uncertainty in inferred mantle potential temperature of $\sim$30–40°C. And this low uncertainty can be generalized to most fertile peridotites because they have MgO and FeO compositions that are similar to KR-4003. In terms of obtaining primary magma MgO and temperature information, the method of calculation is very "forgiving".

[15] Uncertainties in the degree of fertility of a peridotite source also do not propagate to significant errors in MgO for computed primary magmas [*Herzberg et al.*, 2007; *Herzberg and O'Hara*, 2002]. However, peridotite source composition is very important in regulating the amount of melt that can be produced, and all melt fractions calculated with PRIMELT2 are strictly valid for fertile peridotite sources similar in composition to KR-4003 [*Walter*, 1998; *Herzberg and O'Hara*, 2002]. As an example, use of a depleted abyssal peridotite composition with

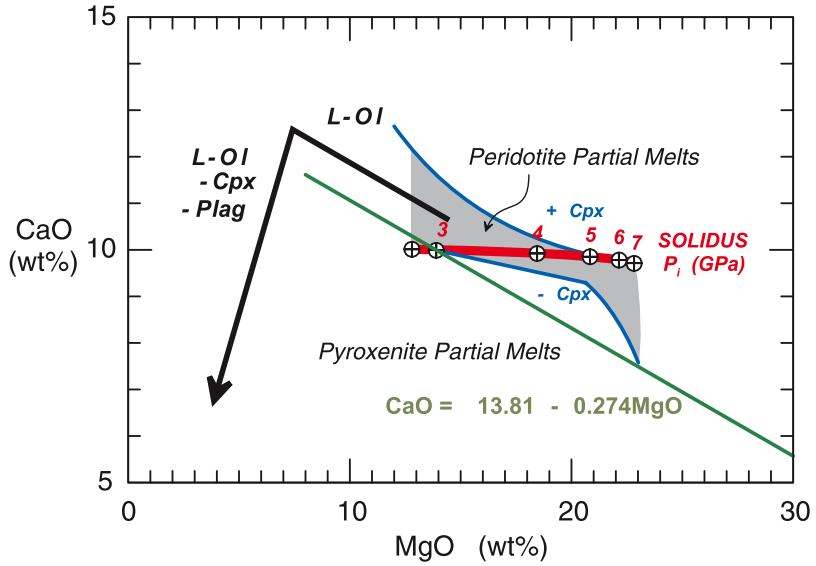

Figure 2. CaO and MgO contents of primary magmas of fertile peridotite produced by accumulated fractional melting. Blue lines define upper and lower CaO filters of these primary magmas and are described by equations (9), (10), and (11) in the text. Lavas with CaO contents lower than those defined by the green line are potential pyroxenite partial melts; they can also be peridotite partial melts that had Cpx removed. Black broken arrow is the typical liquid line of descent for primary magmas that crystallize gabbro in the crust; the drop in CaO often occurs at MgO < ~7–10%. However, Cpx can also crystallize in the mantle and affect magmas with MgO > 10%.

approximately half the Al_2O_3 and CaO content of a fertile peridotite drops the computed melt fraction by more than half [*Herzberg and O'Hara*, 2002]. However, primary magma compositions for the depleted and fertile peridotite compositions differ by only <1.0% MgO for MORB and <0.3% for OIB [*Herzberg and O'Hara*, 2002]. Different peridotite compositions will produce primary magmas with similar MgO at similar conditions of melting, but there is a lesser mass of liquid that can be obtained from depleted peridotite.

3. A Peridotite/Pyroxenite-Source CaO Melting Flag and Filter

[16] The range of MgO and CaO contents for primary magmas produced by accumulated fractional melting is shown in Figure 2, on the basis of experimental results of *Walter* [1998] as modeled by *Herzberg* [2006]. For melting regions beneath old lithospheric mantle, the solidus must be at or above 3 GPa, and therefore all plausible OIB primary melts derived from peridotite sources plot above the green line. Hence the green line separates potential peridotite melts above from pyroxenite-source melts below and takes the form

$$\mathrm{CaO} = 13.81 - 0.274\mathrm{MgO} \qquad (7)$$

[17] Many model pyroxenite-source primary magmas from Hawaii have CaO contents that plot below the line [*Herzberg*, 2006]. Olivine phenocrysts that precipitate from peridotite- and pyroxenite-source melts will therefore have high and low CaO, respectively, in agreement with observations [*Sobolev et al.*, 2005, 2007]. PRIMELT2.XLS alerts the user if the lava composition plots below the green line, indicating a source of error. The incorrect application of PRIMELT2.XLS to lavas that formed from pyroxenite sources will result in MgO contents that are typically too high by 2–3% and potential temperatures that are ~50–70°C too high. This problem is not unique to PRIMELT2.XLS; it is common to all methods that reconstruct primary magmas by addition of olivine to lavas that were derived from primary magmas that separated from olivine-free residues.

[18] Experimental work shows that it is possible that some pyroxenite-source primary magmas can have high CaO contents that are similar to those of peridotite-source lavas [*Kogiso and Hirschmann*, 2001, 2006; *Hirschmann et al.*, 2003; *Kogiso et al.*, 2003; *Keshav et al.*, 2004]. The pyroxenites in these experimental studies are similar in composition to many pyroxenites that have been interpreted to have been crystal cumulates that precipitated deep within the mantle [*Irving*, 1980; *Frey*, 1980; *Sen*, 1988; *Keshav et al.*, 2007]. One reason for

high CaO contents in the experimental liquids is because the pyroxenite compositions chosen in these studies have much higher CaO than pyroxenites that are produced by the reaction of siliceous eclogite-derived melts with peridotite, commonly viewed as a source for some OIB [*Sobolev et al.*, 2005, 2007; *Herzberg*, 2006]. We view the experimental high CaO pyroxenites with suspicion as sources for OIB, but if indeed they are then equation (7) will not be adequate in distinguishing them from peridotite-source lavas. Nevertheless, we have tested whether PRIMELT2 erroneously models these as primary magmas of peridotite. We have assumed that the liquid compositions produced in this pyroxenite-source experimental database are similar to some OIB, and to these we have applied PRIMELT2. Results yielded no successful solutions. In most cases, PRIMELT2 detected these as peridotite-source primary magmas that were modified by clinopyroxene addition or subtraction, as described in section 5 below. In other cases, potential peridotite-source primary magmas had internally inconsistent contents of MgO-CaO and MgO-FeO (see Appendix A3). These tests indicate that, if indeed some high CaO OIB are formed by pyroxenite melting, then application of PRIMELT2 to these samples will not provide erroneous, apparently successful solutions.

[19] It may be possible at some point to incorporate NiO as a flag for peridotite melting in PRIMELT. NiO abundances in many olivine phenocrysts are higher than those expected as precipitates from melts of peridotite-sources [*Sobolev et al.*, 2005, 2007]. However, this interpretation is not necessarily unique because peridotite-source melts can also be high in NiO when orthopyroxene is produced at the expense of olivine owing to reaction with dacitic melts [*Kelemen et al.*, 1998]; in other words it is unnecessary for such reactions to proceed all the way to olivine-free sources in order to yield high-Ni melts.

[20] Finally, we note that OIB with the highest reported ^{3}He/^{4}He have been associated with peridotite sources [*Albarède*, 2008; *Jackson et al.*, 2008]. Indeed, lavas from Iceland, Samoa, and Hawaii reported by *Jackson et al.* [2008] with the highest ^{3}He/^{4}He also have high CaO contents that plot above the green line in Figure 2, consistent with the peridotite source interpretation. One sample from the Galápagos plots slightly below it, but this is similar to others from Fernandina in being low in MgO owing to the effects of crustal Cpx fractionation. It remains to be determined whether peridotite-source lavas inferred from CaO are generally high in ^{3}He/^{4}He. We can imagine various possibilities associated with the mixing of peridotite- and pyroxenite-source lavas.

4. A Volatile-Source CaO Melting Flag and Filter

[21] Many oceanic islands basalts have very low SiO_2 and high CaO owing to low degrees of melting of carbonated peridotite. *Dasgupta et al.* [2007] provided a calibration of the effects of variable CO_2 at 3 GPa, and their results are shown in Figure 3. Their CaO and SiO_2 contents at 0% CO_2 are in good agreement with the anhydrous peridotite parameterizations of *Herzberg* [2004, 2006]. Addition of CO_2 can produce partial melts at very low temperatures and low mass fractions with substantially lower SiO_2 and elevated CaO compared to anhydrous peridotite. As shown below, lavas from the Canary Islands are a good example, trending in a manner that is coincident with the CO_2 array in Figure 3. What is important for our purposes is that these low-temperature carbonated melts can have very high MgO and FeO contents [*Dasgupta et al.*, 2007] which, when normalized to a volatile-free basis, could be erroneously interpreted as high-temperature melts produced from a hot mantle source. Consider, for example, run number A486 in the experiments of *Dasgupta et al.* [2007], at 3 GPa and 1400°C. This temperature is about the same as that of ambient mantle below oceanic ridges at 3 GPa, which would normally produce MORB with about 11% MgO. However, the melt in this experiment contains ~17% CO_2 and, when normalized to a carbonate-free composition, it contains 19.6% MgO and 11.6% FeO. If this were a naturally occurring lava, the MgO content would indicate a potential temperature of about 1550°C instead of 1350°C, an error of 200°C. We clearly need to exclude this type of ambiguity, and this is possible because the carbonated peridotite melt is also high in CaO and low in SiO_2 compared to partial melts of anhydrous peridotite. These melts plot to the left of the green line in Figure 3, which is described by the equation

$$\mathrm{CaO} = 2.318\mathrm{SiO_2} - 93.626 \quad (8)$$

and located to pass through the model anhydrous peridotite solidus composition at 5 GPa. This filter will erroneously exclude accumulated melts from melting regimes with final pressure greater than or equal to 5 GPa, but this is deeper than the base of

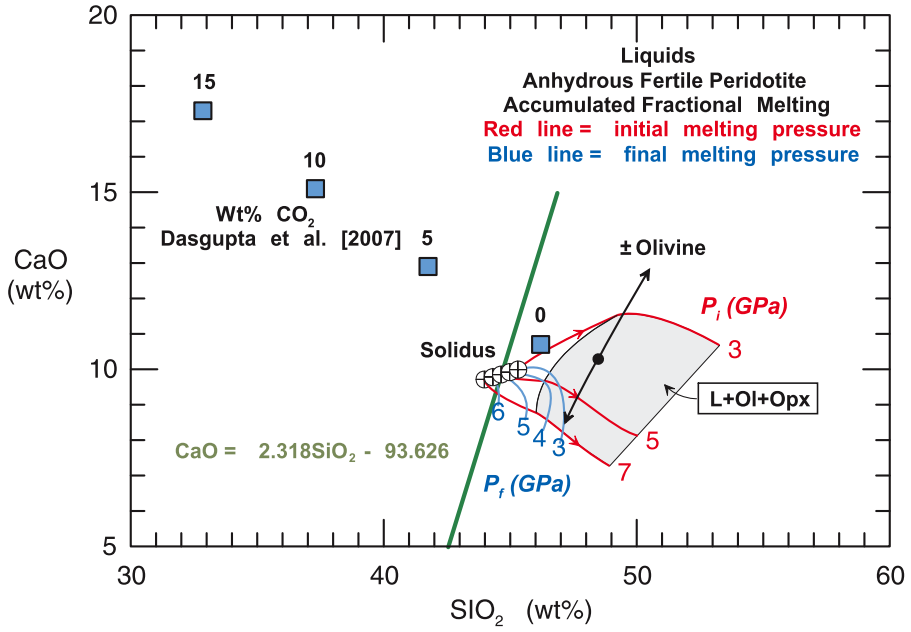

Figure 3. CaO and SiO_2 contents of primary magmas of carbonate-bearing [*Dasgupta et al.*, 2007] and carbonate-free fertile peridotite [*Walter*, 1998; *Herzberg*, 2004, 2006]. The green line is an approximate filter that separates CO_2-enriched and deficient lavas and is described by equation (8) in the text.

any oceanic lithosphere. The position of the green line is approximate because there is a considerable range in the reported CaO and SiO_2 contents of experimental partial melts at elevated CO_2 [*Dasgupta et al.*, 2007]. PRIMELT2 provides a warning if a primary magma solution is attempted for a lava composition that plots to the left of the green line in Figure 3. All primary magmas modeled with PRIMELT2 and reported below have been made on lava compositions that plot to the right of the green line in Figure 3. This problem is not unique to PRIMELT2. It is common to all methods that reconstruct primary magmas without due consideration to volatile effects.

[22] It is important to note that there are few comparable data on the effects of H_2O. Some high-pressure data plot to the left of the green line, similar to that of CO_2 [*Kawamoto and Holloway*, 1997], and others plot to the right [*Jakobsson and Holloway*, 2008]. A detailed calibration is currently in progress (M. M. Hirschmann, personal communication, 2008).

5. Clinopyroxene Fractionation CaO Flag and Filter

[23] When clinopyroxene is fractionated in the crust, it often crystallizes together with olivine [L + Ol + Cpx] or olivine and plagioclase [L + Ol + Cpx + Plag]. This usually occurs after the primary magma has evolved to a derivative liquid with MgO below the 7–10% range [*Herzberg et al.*, 2007]. When this occurs, Cpx removal lowers the CaO content of the differentiated magmas as shown by the black arrow in Figure 2. That is, there is a break in the LLD, and this is easily identified in a suite of lavas. It is possible to back track the effects of clinopyroxene fractionation, but this is difficult to do properly and adds a new layer of uncertainty. As PRIMELT2 reconstructs primary magmas by addition and subtraction of olivine only, it cannot be applied to highly fractionated magmas that lost augite and are low in CaO. These derived liquids are also high in FeO, and the incorrect application of PRIMELT2 to such a lava will result in primary magma compositions that are too high in MgO [*Herzberg et al.*, 2007]. This problem is not unique to PRIMELT2. Any method that reconstructs primary magmas by addition of olivine to lavas that have also lost augite and/or plagioclase will yield MgO contents and inferred source temperatures that are too high [*Herzberg et al.*, 2007].

[24] Clinopyroxene can also accumulate in the mantle [*Irving*, 1980; *Frey*, 1980; *Sen*, 1988; *Albarède et al.*, 1997; *Keshav et al.*, 2007], from primary or derivative liquids having high MgO. Deep crystallization of high CaO augite can have the same effect as shallow augite fractionation on

the CaO contents of high MgO primary magmas, and can yield mantle potential temperatures that are too high. Precipitation is likely to occur in the lithosphere during melt transit [*Albarède et al.*, 1997] rather than in the melting region, and the clinopyroxenes will have high CaO [*Irving*, 1980; *Frey*, 1980; *Sen*, 1988; *Keshav et al.*, 2007]. Clinopyroxenes within the peridotite melting region often have low CaO contents, the 6–10% range [*Herzberg and Zhang*, 1996; *Longhi and Bertka*, 1996; *Longhi*, 2002; *Walter*, 1998]. However, these may not be a player for several reasons. First, they will melt out in the melting region rather than precipitate. And, peridotite-source melts that intermingle with any high silica pyroxenite source melts in the melting region are expected to precipitate high CaO clinopyroxene instead. Precipitation rather than mixing is an unexpected consequence of melts having compositions on the low- and high-SiO_2 side of the garnet-pyroxene plane, which is a thermal divide at high pressures [*O'Hara and Yoder*, 1967; *Herzberg*, 2006].

[25] PRIMELT2 evaluates the potential effects of high-CaO augite fractionation in high-MgO magmas using the range of CaO and MgO contents of accumulated fractional melts of fertile peridotite. These melt compositions have been modeled assuming the mixing of fractional melts occurs strictly in the vertical streamline [*Herzberg*, 2006]. For example, an accumulated fractional melt is produced by the mixing of instantaneous fractional melts that are generated by decompression from an initial to a final melting pressure, 5 GPa and 2 GPa for example. The accumulated melt is isolated from and does not mix with another accumulated melt from an adjacent vertical streamline. In reality, accumulated melts from different vertical streamlines might mix by melt focusing or by mixing in a plume with a conduit that is tilted or flattened as it spreads at the base of the lithosphere. These scenarios are expected to broaden the range of possible primary magma compositions. The results shown in Figure 2 are mostly vertical streamline compositions given by *Herzberg* [2006], but marginally widened to include the possible mixing of vertical streamline melts in 3 to 5 GPa range; the resulting filter remains conservative, more likely to flag a primary melt with an unmodeled mixing path than to fail to flag a liquid that experienced some augite fractionation.

[26] When a primary magma has been modified by addition of augite, the magma will have too much CaO and may plot above the upper blue curve in Figure 2. PRIMELT2 alerts the reader to this possibility using the following equation for the upper blue curve:

$$\mathrm{CaO} = 1.095 + 0.154\mathrm{MgO} + 116.58/\mathrm{MgO} \qquad (9)$$

[27] When a primary magma has been modified by subtraction of augite, the magma will be deficient in CaO and may plot below the lower blue curve in Figure 2. PRIMELT2 alerts the reader to this possibility using the following two equations for segments of the lower blue curve:

$$\mathrm{CaO} = 11.436 - 0.104\mathrm{MgO} \qquad (10)$$

if the MgO content is <20.6% and

$$\mathrm{CaO} = -23.209 + 3.643\mathrm{MgO} - 0.1\mathrm{MgO}^2 \qquad (11)$$

if the MgO content is >20.6%.

[28] There are 89 lava samples from Mauna Kea that plot above the green line in Figure 2, and these qualify as olivine-fractionated derivatives of peridotite-source primary magmas. However, only 19 of these have primary magmas that actually plot between the blue lines in Figure 3, indicating that the majority of these lavas have been affected by clinopyroxene fractionation. The size of the error that can arise when Cpx fractionation is not considered can be seen in Figure 4. Some primary magmas for Mauna Kea lavas have about 18% MgO, and the ones indicated by $Fe_2O_3/TiO_2 = 0.5$ are most relevant as discussed immediately below. Loss of Cpx yields lavas that are low in CaO and high in FeO. PRIMELT2 calculates the primary magmas anyway, but alerts the reader that they are too low in CaO, using equations (10) and (11). These model primary magmas, low in CaO and high in FeO, are also too high in MgO, up to 22%. The effect of Cpx fractionation can therefore produce an error of 4% MgO (absolute) in the calculation of a primary magma composition, and this propagates to a potential temperature that can be 100°C too high.

6. Fe_2O_3 in OIB

[29] All estimates of primary magma composition require knowledge of the Fe_2O_3 and FeO contents of the lava. It is the exchange of FeO and MgO between liquid and olivine that permits this reconstruction to be made, as revealed in equations (1)–(3). However, it is the total iron content of a lava is typically obtained by X-ray fluorescence analysis

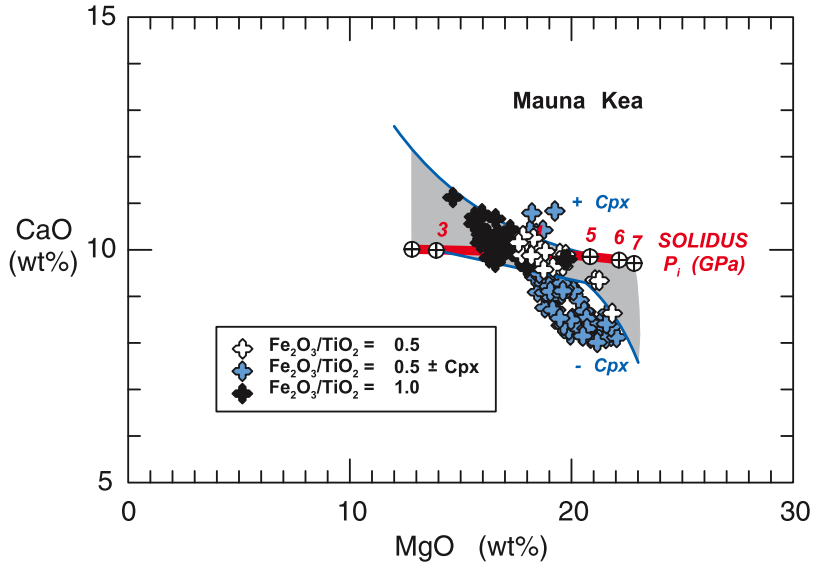

Figure 4. CaO and MgO contents of peridotite-source primary magmas from Mauna Kea, Hawaii, calculated by PRIMELT2 from lava analyses in GEOROC. White crosses, successful primary magmas calculated with Fe_2O_3/TiO_2 = 0.5 and Fe^{2+}/Fe^{total} = 0.91–0.93, similar to those determined analytically [*Rhodes and Vollinger*, 2005]. Blue crosses, unsuccessful primary magma solutions in that they have CaO contents outside the bounds imposed by the Cpx fractionation filters (i.e., blue lines) and are not reliable primary magmas. Black crosses, successful primary magma solutions calculated with Fe_2O_3/TiO_2 = 1.0, but they have Fe^{2+}/Fe^{total} = 0.80–0.86, lower than analytical determinations [*Rhodes and Vollinger*, 2005].

and reported as Fe_2O_3. In most cases it is assumed that $Fe^{2+}/Fe^{total} \cong 0.9$, but PRIMELT2 allows this to be an adjustable parameter by providing a cell that requires the input of Fe^{2+}/Fe^{total}.

[30] Circumstantial evidence for elevated Fe_2O_3 in some OIB is revealed in the FeO_T-MgO liquid line of descent. For example, MORB displays a strong enrichment in FeO_T when plagioclase and augite crystallize with olivine because FeO is incompatible and most of the iron is FeO (Figure 5a). However, a reversal occurs when FeO_T begins to drop for MgO $\leq$ 4% along the LLD owing to oxide (magnetite or ilmenite) crystallization. The form of this FeO_T-MgO LLD, with a well-developed negative correlation throughout most of the MgO range, is seen also for lavas from Hawaii (Figure 5a), Iceland, and the Galápagos Islands. But it is not observed in other OIB. Lavas from the Canary Islands display no enrichment in iron (Figure 5b), and there is a greater range of FeO_T at any given MgO content. The case for the Canary Islands is similar to most lavas from Azores, Cape Verde, Cameroon, Cook-Austral, Juan Fernandez, Marquesas, Reunion, St. Helena, Samoa, Society, Pitcairn-Gambier, and Tristan da Cunha. For the latter group of OIB, the FeO_T-MgO LLD appears similar of those for subduction-related lavas (Figure 5b), presumed to form in a more oxidizing environment [*Carmichael*, 1991]. Using PRIMELT2, we examine more carefully the assumption that Fe^{2+}/Fe^{total} is constant and near 0.9, and find evidence that some OIB might indeed be more oxidizing. This is consistent with the petrographic observation of an abundance of early Fe-Ti oxide phenocrysts in lavas from the Canary Islands [*Hoernle*, 1987]. For a given analysis of total Fe, higher Fe_2O_3 requires that there be less FeO, which propagates to a primary magma with lower MgO contents and lower source temperatures [*Herzberg et al.*, 2007].

[31] Although the partitioning of Fe^{3+} between crystals and melts has not been determined experimentally, we can assume that it behaves mostly as an incompatible element in silicate phases. This is presumably the reason for the reversal of FeO_T in the MORB LLD (Figure 5a); Fe_2O_3 is incompatible during fractionation until its concentration increases with progressive crystallization to the point that the melts become saturated in magnetite.

[32] Many incompatible lithophile trace elements in OIB are positively correlated [*McKenzie et al.*, 2004]. For example, the ratio Zr in ppm to TiO_2 in weight% is about 67, increasing only for SiO_2-enriched compositions that ultimately become zircon-saturated. By analogy to such observations, and given the expected incompatible behavior of Fe_2O_3, we attempted to define the unmeasured Fe_2O_3

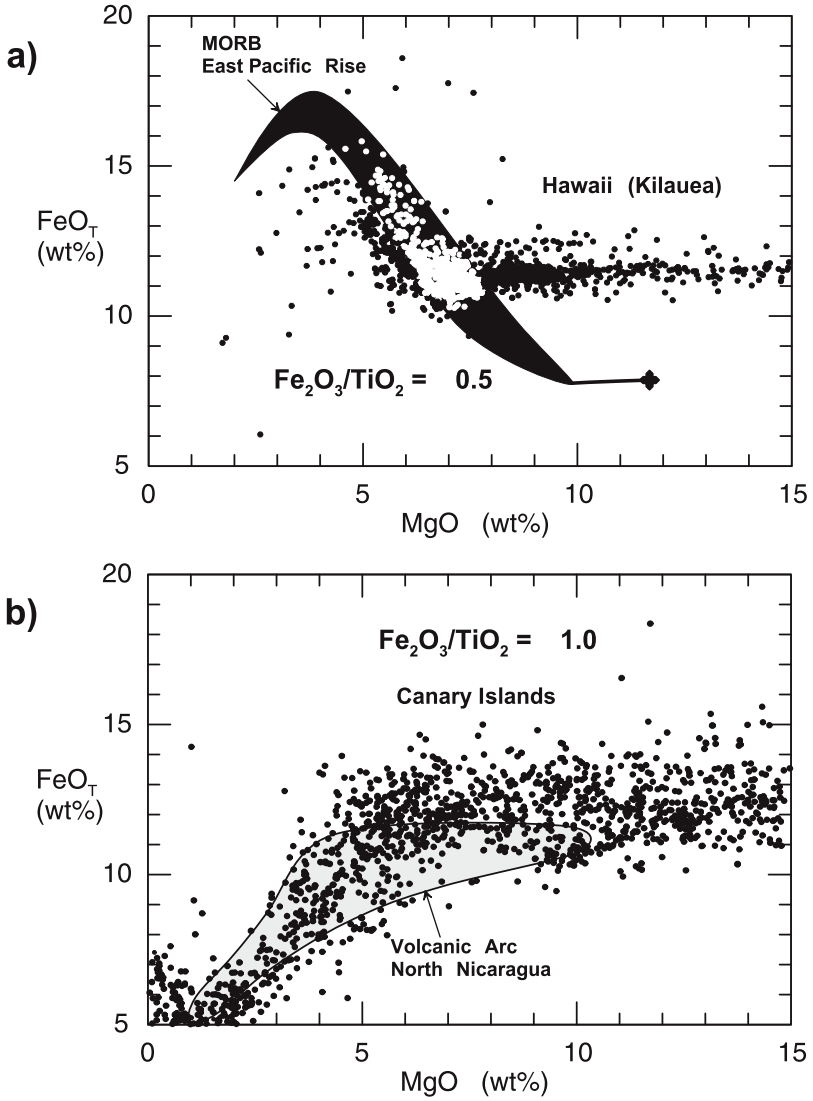

Figure 5. MgO-FeO_T liquid lines of descent. (a) OIB that display FeO_T enrichment are represented here by Hawaii and MORB and also occur at Iceland and the Galápagos Islands. Successful primary magma solutions are obtained for these with Fe_2O_3/TiO_2 = 0.5 and Fe^{2+}/Fe^{total} = 0.91–0.95. (b) OIB that do not display FeO_T enrichment are represented here by the Canary Islands and occur also at the Azores, Cape Verde, Cameroon, Cook-Austral, Juan Fernandez, Marquesas, Reunion, St. Helena, Samoa, Society, Pitcairn-Gambier, and Tristan da Cunha. Successful primary magma solutions are obtained for these with Fe_2O_3/TiO_2 = 1.0 and Fe^{2+}/Fe^{total} = 0.75–0.91. OIB whole rock and glass analyses are from GEOROC (http://georoc.mpch-mainz.gwdg.de/georoc/), EPR glass analyses are from PETDB (http://www.petdb.org/), and the Nicaraguan database is from *Carr et al.* [2003].

contents of OIB lavas by assuming a fixed Fe_2O_3/TiO_2 ratio. We have found that by adjusting Fe^{2+}/Fe^{total} in PRIMELT2 so that the primary magma has Fe_2O_3/TiO_2 = 0.5, we calculate primary magmas for Mauna Kea with Fe^{2+}/Fe^{total} = 0.91–0.93, similar to those determined analytically by *Rhodes and Vollinger* [2005] on lavas from Mauna Loa. They contain 17–22% MgO, and are shown in Figure 4. Successful primary magma solutions are also obtained by assuming Fe_2O_3/TiO_2 = 1.0, but these have Fe^{2+}/Fe^{total} = 0.80–0.86 (lower than analytical determinations) and 15–20% MgO (Figure 4), or about 2% absolute too low in MgO. PRIMELT2.XLS offers the option of fixing Fe_2O_3/TiO_2 and calculating Fe^{2+}/Fe^{total} from this constraint; in the case of OIB lavas for which only total Fe is known and that display enrichment in FeO_T along the LLD, we recommend fixing Fe_2O_3/TiO_2 = 0.5 (Figure 5a).

[33] We now examine Fe_2O_3 in OIB that do not display enrichment in FeO_T (Figure 5b), using lava

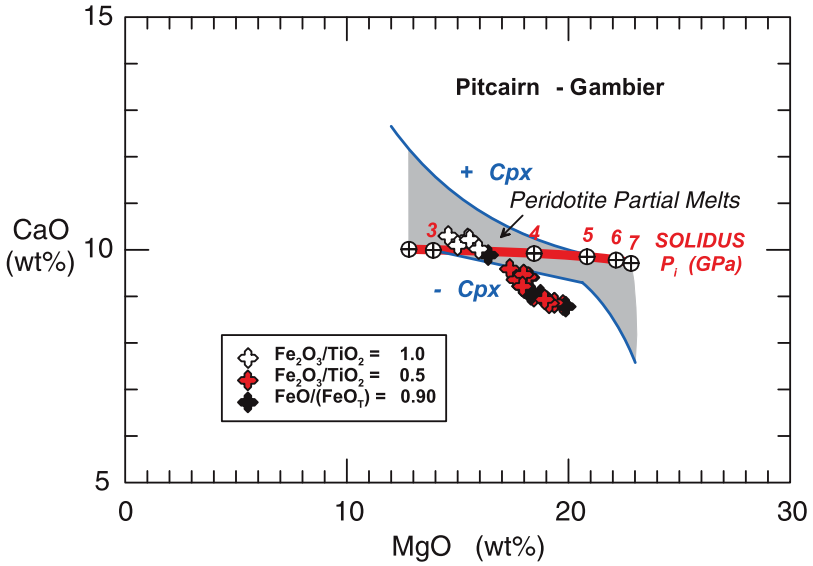

Figure 6. CaO and MgO contents of peridotite-source primary magmas from Pitcairn-Gambier calculated by PRIMELT2, from lava analyses in GEOROC. White crosses, successful primary magmas calculated with Fe_2O_3/TiO_2 = 1.0. Red crosses, unsuccessful primary magma solutions calculated with Fe_2O_3/TiO_2 = 0.5. Black crosses, mostly unsuccessful primary magma solutions calculated with Fe^{2+}/Fe^{total} = 0.90. Pitcairn is representative of other OIB that display no enrichment in FeO_T (Figure 5b).

compositions from Pitcairn-Gambier as a representative example. Setting the parameter Fe_2O_3/TiO_2 = 0.5 yields magmas with Fe^{2+}/Fe^{total} = 0.90 – 0.96, similar to some Hawaiian lavas, but these have CaO contents that are too low to be primary magmas (Figure 6). Similarly, primary magmas calculated from the assumption that the lavas have Fe^{2+}/Fe^{total} = 0.90 are also too low in CaO. In contrast, successful primary magma solutions in MgO-CaO space (Figure 6) are obtained for a more oxidizing condition, with Fe_2O_3/TiO_2 = 1.0 and Fe^{2+}/Fe^{total} = 0.79–0.91. This example is typical: like Pitcairn-Gambier, all other OIB that do not display FeO_T enrichment (Figure 5b) also yield successful primary magma solutions with Fe_2O_3/TiO_2 = 1. It is noted that successful primary magma solutions must also be internally consistent in all major elements, and results seen in MgO-CaO agree well with MgO-FeO, MgO-SiO_2, and multicomponent projection space (see diagrams and discussion for Figure A1 by *Herzberg et al.* [2007]). The issue of internal consistency is discussed in Appendix A3.

[34] PRIMELT2 modeling indicates that there may be a reduced and an oxidized population of OIB, as summarized in Figure 7a. The reduced and oxidized groups are well-separated and are characterized by Fe^{2+}/Fe^{total} > 0.9 and ~0.75–0.85, respectively. We would be surprised if there were no intermediate possibilities, and recommend that this be subjected to closer examination. At present, the only wet chemistry data that have been reported are those on the reduced group [*Wright et al.*, 1975; *Rhodes and Vollinger*, 2005]. The existence of a category of oxidized OIB with Fe_2O_3/TiO_2 = 1.0 can be tested and falsified by wet chemistry performed on lavas from the Azores, Canary Islands or any other members of the oxidized group in Figure 7a. Should these samples also display Fe^{2+}/Fe^{total} > 0.90, rather than ~0.75–0.85 as we suggest here, then the following implications would hold: (1) the MgO contents and potential temperatures computed here would be too low, and (2) either the CaO contents of peridotite primary magmas shown in Figure 2 are not generally applicable to all cases of peridotite partial melting or all these apparently oxidized OIB lavas have either been affected by augite fractionation or a component of pyroxenite-source melting.

[35] The ratio Fe^{2+}/Mn is typically <60 in experimental melts of anhydrous peridotite [*Walter*, 1998; *Liu et al.*, 2008] and their parameterizations [*Herzberg*, 2004]. In contrast, experimental melts of pyroxenite have Fe^{2+}/Mn > 60 [*Liu et al.*, 2008]. Olivine phenocrysts that precipitate from peridotite- and pyroxenite-source melts will therefore have low and high Fe^{2+}/Mn, respectively, in agreement with observations [*Sobolev et al.*, 2005, 2007]. This creates the potential for using Fe^{2+}/Mn to further constrain the oxidation state of OIB

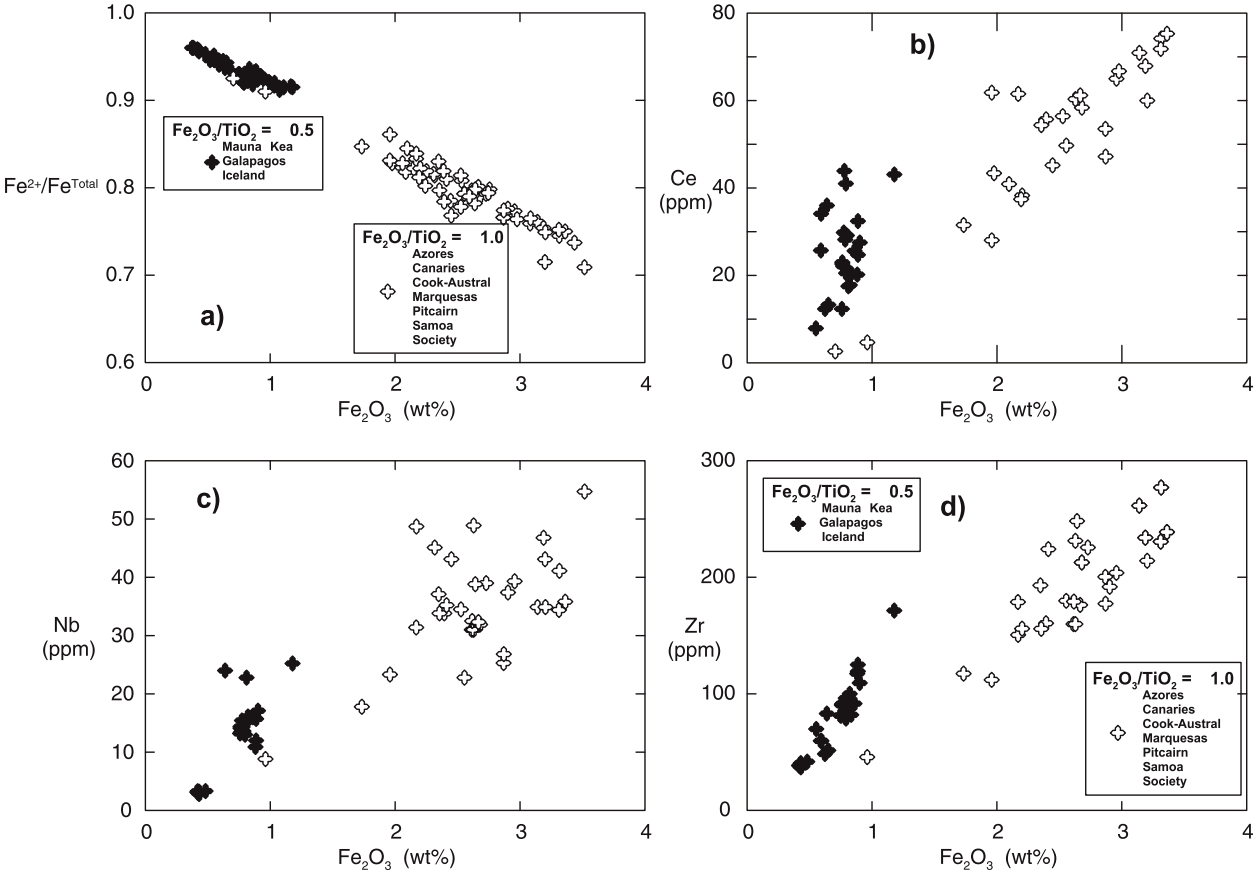

Figure 7. Summary of Fe_2O_3 and various incompatible trace element abundances in primary magmas for the OIB occurrences listed. Fe_2O_3/TiO_2 is assumed to be 0.5 and 1.0 for reduced and oxidized OIB, respectively. Primary magmas are calculated with PRIMELT2, from lava analyses in GEOROC.

lavas. Our model yields $Fe^{2+}/Mn < 60$ in 80% of the cases examined, in general agreement with experimental measurements.

[36] Assumptions about Fe^{2+}/Fe^{total} clearly propagate to significant variations in MgO and FeO, and errors in the inferred mantle potential temperature. For Pitcairn, the reduced model yields MgO in the 17–20% range, much higher than 14–16% MgO in the oxidized model (Figure 6). The higher MgO content would propagate to a source with a potential temperature of 1520–1570°C, in contrast to 1450–1480°C for the preferred oxidizing model. This 70–90°C uncertainty in T_P is similar to the ~100°C global range for ambient mantle that melts to produce MORB [*Herzberg et al.*, 2007].

7. Trace Elements and Volatiles in OIB Primary Magmas

[37] The reporting of Ce, Nb, and Zr in OIB lavas in GEOROC permits an estimate of their concentrations in primary magmas by solving the equation for fractional crystallization [*Shaw*, 1970] wherein the partition coefficients with respect to olivine are assumed to be zero. Results shown in Figures 7b, 7c, and 7d demonstrate positive correlations with respect to Fe_2O_3 for the OIB population as a whole. Of course, these are an expected consequence of our assumption that Fe_2O_3 and TiO_2 are positively correlated because many trace elements correlate with TiO_2, especially those with similar partition coefficients. Nevertheless, this evidence encourages more work to be done on understanding the magmatic fractionation of Fe^{2+} and Fe^{3+}, as indicated also by iron isotopes [*Weyer and Ionov*, 2007; *Teng et al.*, 2008].

[38] OIB lavas are generally degassed upon eruption and it can be difficult to determine the concentration of volatile components in observed lavas, which makes it challenging to infer volatile contents of their primary magmas or mantle sources. However, it has been observed in MORB suites and in rare undegassed OIB samples that $H_2O/Ce \sim 200$ [*Dixon et al.*, 2002]. CO_2/Nb has

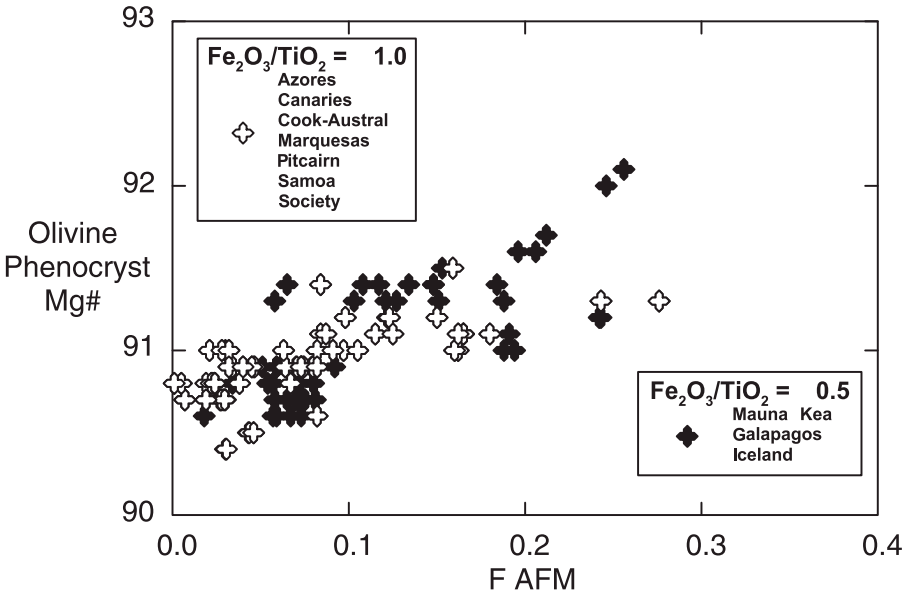

Figure 8. Calculated olivine phenocryst compositions of primary magmas for the OIB occurrences listed in Figure 7.

been estimated to be 239 and 530 by *Saal et al.* [2002] and *Cartigny et al.* [2008], respectively. These ratios allow inference of H_2O and CO_2 contents from literature data on Ce and Nb. The calculated Ce and Nb contents of the primary magmas in Figure 7 lead to estimates that the more reducing primary OIB contain ~0.2–0.4% H_2O and ~0.1–1.0% CO_2. The more oxidizing primary OIB are more volatile-rich, with ~0.6–1.6% H_2O and ~0.2–3.0% CO_2. In the Azores, the hottest and driest primary magmas formed at FAFM = 0.07 and contain 43 ppm Ce. Using a partition coefficient of 0.01 for water, this indicates a source with ~600 ppm H_2O, similar to 700 ppm H_2O modeled for MORB from the Mid-Atlantic Ridge near the Azores [*Asimow et al.*, 2004].

[39] It is emphasized that estimated volatile abundances are minimum values because the primary magmas were modeled from lava compositions with SiO_2 contents that plot to the right of the green line in Figure 3 (see discussion in section 4). PRIMELT2 cannot model lava compositions with lower SiO_2 contents, and these are typically carbonate-rich low-degree melts that are elevated in all trace elements.

8. Melt Fraction and Olivine Phenocryst Mg Number

[40] PRIMELT2 differs from other methods of primary magma calculation in that it does not assume or require a prior knowledge of olivine composition [*Herzberg et al.*, 2007]. Rather, it calculates the composition of the olivine phenocryst that would crystallize from the primary magma in the event that it erupts on the surface, using olivine crystallization temperature from *Beattie* [1993] and olivine-liquid Fe-Mg exchange from *Toplis* [2005]. Calculated compositions are given in Figure 8 for the OIB occurrences listed in Figure 7. These typically have Mg Numbers of 90.5–91.5, in good agreement with observed maxima in olivine phenocryst populations [e.g., *Herzberg et al.*, 2007]. There is a significant positive correlation with melt fraction F for accumulated fractional melting (Figure 8), as expected from the increasing Mg number in residual peridotites with increasing degree of melt extraction.

9. Melt Fractions in the Mauna Kea and Galápagos Sources: Hot Spots

[41] FeO and MgO contents and melt fractions of primary magmas formed by accumulated fractional melting are shown in Figure 9a, computed from equations (1) to (3). Pressures of initial and final melting indicated by red and blue contours, respectively, are parameterizations of experimental data [*Walter*, 1998; *Herzberg and O'Hara*, 2002; *Herzberg*, 2004; *Herzberg et al.*, 2007]. Also shown are primary magmas calculated using PRIMELT2 for Mauna Kea and the Galápagos Islands. We specifically focus on these two OIB

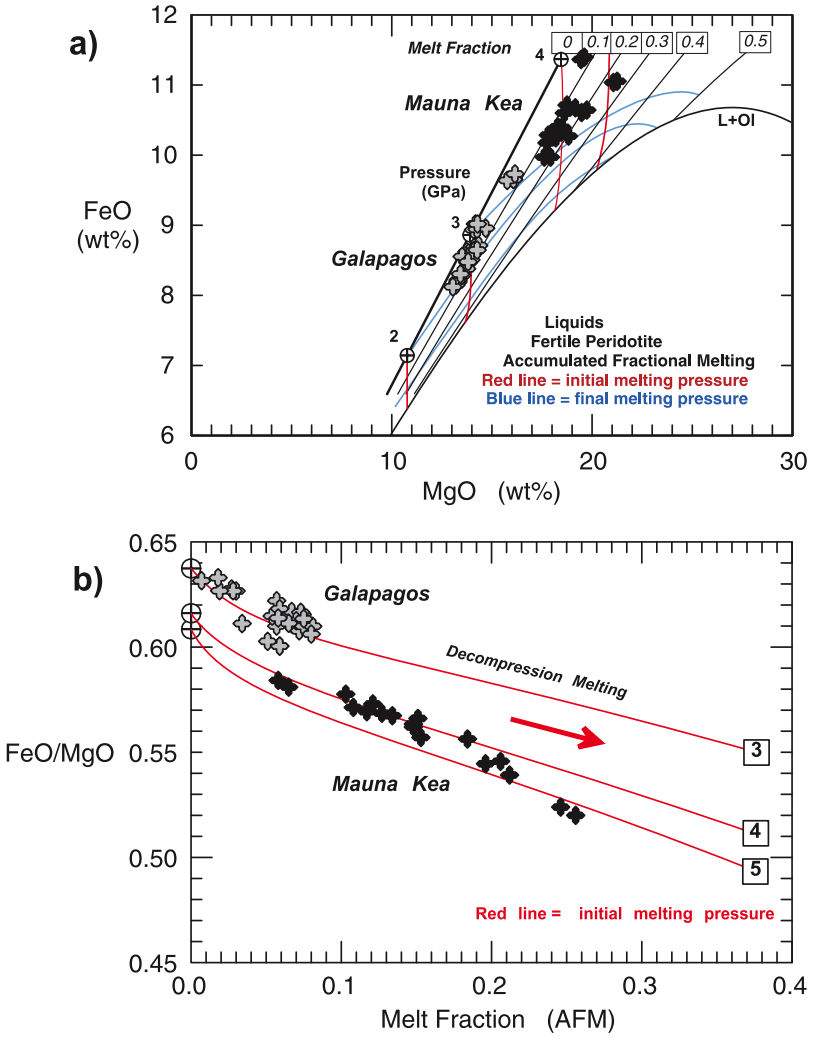

Figure 9. Iron-magnesium relations for primary magmas from Mauna Kea and the Galápagos Islands. (a) Melt fractions at specific values for FeO and MgO are calculated from equations (1) to (3). Crosses, successful primary magma solutions from PRIMELT2, calculated with Fe_2O_3/TiO_2 = 0.5. Red and blue lines, initial and final melt pressures, respectively. Note the limited range of MgO with increasing melt fraction and constant FeO content. Note also the even smaller range in MgO that attends decompression. (b) Results from Figure 9a, but with a better representation of melt fraction.

occurrences because of the limited geographical distribution from which the lavas were sampled. For Galápagos, the melt fraction ranges from ~0 to 0.08. For Mauna Kea the melt fraction ranges from 0.05 to 0.25. The lavas from Mauna Kea come from both shield and post-shield types, which range in age from about 232 to 484 Ka [*Eisele et al.*, 2003]. During this length of time, the lithosphere would have moved about 20 km over the Mauna Kea source, on the basis of a plate velocity of 8.3 cm/a. This reasoning suggests that, for a steady melting region in time, sampled spatially by plate motion, melt fractions of 0.05 to 0.25 were produced in the Mauna Kea source over a horizontal distance of only 20 km. Such large variations in melt fraction produced over short horizontal distances are difficult to reconcile with a long-wavelength thermal anomaly in ambient mantle [*Anderson*, 2000]. Rather, it points to a spatially limited source of heat and magmatism, a hot spot.

[42] Decompression melting begins at some initial pressure and ends at a final pressure that is generally determined by some boundary like the lithosphere-asthenosphere boundary. When melting occurs up a vertical streamline, the melt fraction is highest at the final melting pressure (Figure 9a). For Mauna Kea and Galápagos, these final melting pressures were >3 and >2 GPa, respectively. The lithosphere below Hawaii is thicker because it is

older, consistent with its large distance from the spreading center where Pacific lithosphere is being made.

[43] Major melting begins at the anhydrous solidus, and this occurs at higher pressures below Hawaii compared to Galápagos (Figure 9a). Melting always begins deeper when the source is hotter, and this produces primary magmas with a higher MgO content, as discussed below. It is important to note, however, that there need not be a relationship between T_P and melt fraction. Hot mantle sources will not produce much melt if the pressure of final melting is high (Figure 9a).

10. OIB Mantle Potential Temperatures: More Hot Spots

[44] The temperature at which olivine crystallizes from a magma depends mainly on the MgO content in weight % and the pressure (GPa), and can be calculated from

$$T(^\circ C) = 935 + 33MgO - 0.37MgO^2 + 54P - 2P^2 \quad (12)$$

[*Herzberg and O'Hara*, 2002; *Herzberg et al.*, 2007; *Beattie*, 1993]. This equation was used to contour the MgO contents of liquids formed by batch melting of fertile peridotite in T-P space [*Herzberg and O'Hara*, 2002, Figure 8a]. Isopleths of MgO are approximately coincident with adiabatic T-P paths of *Iwamori et al.* [1995] and *Asimow et al.* [2001]. For example, batch melts of fertile peridotite contain ~17 ± 1% MgO along an adiabatic gradient having a potential temperature of 1500°C. And isopleths of MgO for batch melts of depleted peridotite are the same. Clearly, equation (12) does not depend on the composition of the peridotite being melted, whether it is fertile or depleted. Therefore, the approximate T-P coincidence of an MgO isopleth and an adiabatic melting path holds true even for the case of fractional melting wherein the peridotite source composition becomes more depleted during melt removal. It is for this reason that the MgO content of an accumulated fractional melt does not change greatly as melting progresses during decompression in all petrological models [*Langmuir et al.*,1992; *Longhi*, 1992, 2006; *Herzberg and O'Hara*, 2002; *Herzberg et al.*, 2007]. From a computational point of view, this approximation greatly simplifies our ability to infer mantle potential temperature from the MgO content of a primary magma, and PRIMELT2 provides inferences about mantle potential temperature that is quite similar to other methods [*Courtier et al.*, 2007].

[45] The mantle potential temperature T_P is simply the metastable extension to the surface of the adiabat from the solid convecting part of mantle at depth [*McKenzie and Bickle*, 1988]. The primary magma MgO content along an adiabatic melting T-P path, as given by equation (12), can now be related to the adiabatic path in the solid region as defined by T_P of *Iwamori et al.* [1995] using the equation

$$T_P(^\circ C) = 1463 + 12.74MgO - 2924/MgO \quad (13)$$

as given also by *Herzberg et al.* [2007]. Once a primary magma has been calculated by PRIMELT2, its MgO content is used to infer T_P using equation (13). Results for the OIB cases considered here are shown in Figure 10.

[46] An important observation in Figure 10 is the range of T_P for each occurrence. Again we focus on Galápagos and Mauna Kea because the lava samples come from a limited geographical distribution and the melt fractions vary greatly as discussed in section 9. Within the Galápagos Archipelago, T_P = 1400–1500°C, and samples collected from the 20 km diameter island of Floreana display T_P that varies from 1420 to 1490°C. The lower T_P end of the spectrum extends into the region more characteristic of ambient mantle below the nearby Galápagos spreading center. This is seen also for the Canaries, Society, Samoa, and the Azores, which displays some of the lowest potential temperatures of all OIB. Those samples from the Azores that display the lowest T_P also have the highest $^{143}Nd/^{144}Nd$, indicating increasingly MORB-like source compositions as well as potential temperatures. The ~100°C T_P variation in one 20 km island in the Galápagos is comparable to the ~100°C variation below the 65,000 km global network of oceanic ridges that produce MORB. Horizontal gradients in potential temperature in units of °C/km are about 5 for Galápagos and Mauna Kea sources and about 10^{-3} for MORB sources. We argue that these high horizontal temperature gradients are most consistent with a plume-source model for oceanic hot spots.

[47] For Mauna Kea, constructed during ~20 km of lithospheric plate movement, T_P varies from 1520 to 1600°C. It is not clear why samples produced from lower potential temperatures are not observed. One possibility is that the T_P range is actually based on primary magmas that were in

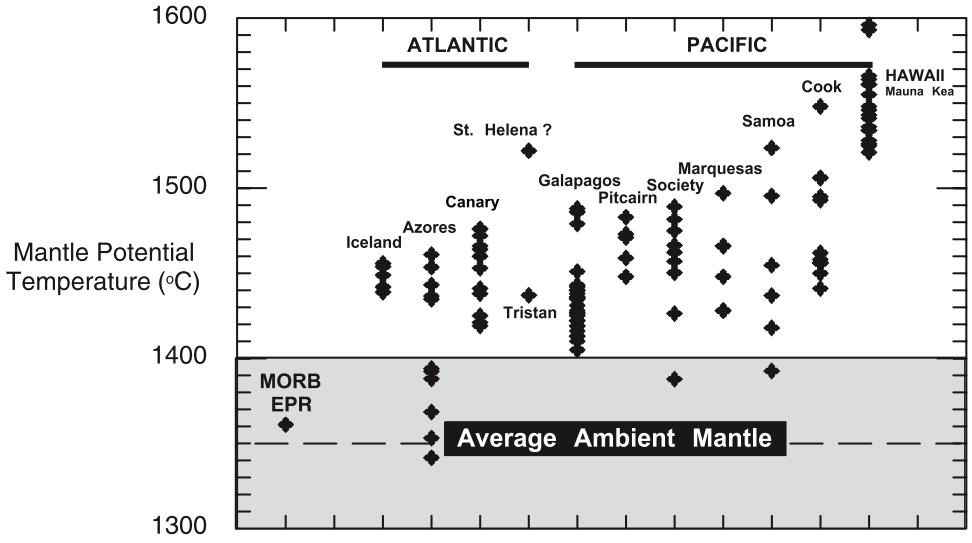

Figure 10. Summary of mantle potential temperatures (T_P) for oceanic islands, calculated from OIB lava compositions using PRIMELT2.

fact mixtures of those with a wider MgO range; the 1520–1600°C range may then be a mean of lower and higher T_P. This scenario might happen if melts from the axial and peripheral streamlines mix as the mantle plume conduit impacts the base of the lithosphere [*Ribe and Christensen*, 1999].

[48] Of all the OIB investigated with PRIMELT2, Hawaii is the hottest. Owing to the range in T_P for each occurrence, it is appropriate to refer to T_P maxima, which are generally higher in the Pacific compared to those in the Atlantic. An exception might be St. Helena, but this estimate is based on one sample and should be reproduced by further sampling before it is accepted with confidence. The oceanic island nearest to St. Helena for which a T_P estimate can be made is Tristan da Cunha, and it has a low T_P (Figure 10).

11. Hot Spots, Wet Spots, Mantle Fertility

[49] It has been postulated that oceanic islands are magmatically productive because the mantle source is wet or fertile rather than hot [*Bonath*, 1990; *Green and Falloon*, 1998; *Anderson*, 2007]. We examine this conjecture using PRIMELT2 modeling on lavas from the Canaries and Galápagos Islands, which represent oxidized and reduced types, respectively (Figure 7). Mantle potential temperatures for both are about the same, and span the 1400–1500°C range (Figure 10). However, lavas from the Canary Islands are geochemically different as shown by greater trace element enrichments in the oxidized group (Figure 7). Cerium, a proxy for H_2O (section 7), is much more abundant in lavas and primary magmas from the Canaries compared to the Galápagos (Figure 11a), despite the higher melt fractions for the Canaries. Furthermore, most but not all lavas from the Canaries are low in SiO_2 and high in CaO, indicating they formed by variable degrees of carbonated peridotite melting as shown in Figure 11b. In contrast, all peridotite-source lavas from the Galápagos Islands plot to the right of the green line in Figure 11b, indicating a minor role for source volatiles. Clearly, hot spots may or may not be wet. But there is no evidence that the oceanic islands considered here can form by addition of volatiles in the absence of a thermal anomaly.

[50] All conclusions in this paper were drawn from the implementation of PRIMELT2 on lavas that formed by melting a peridotite source. However, it has also been suggested that some oceanic islands might form by melting of metasomatized lithospheric mantle [*Niu and O'Hara*, 2003; *Pilet et al.*, 2005, 2008]. Experiments show that melts of amphibole veins are expected to produce very low SiO_2 lavas [*Pilet et al.*, 2008], and these will be filtered out by PRIMELT2 using equation (8). Reaction of such experimental melts with peridotite at 1.5 GPa elevates SiO_2 [*Pilet et al.*, 2008] but, with one exception, PRIMELT2 will identify these as either melts of pyroxenite or volatile peridotite. We acknowledge the important possibility that metasomatized lithospheric mantle might be

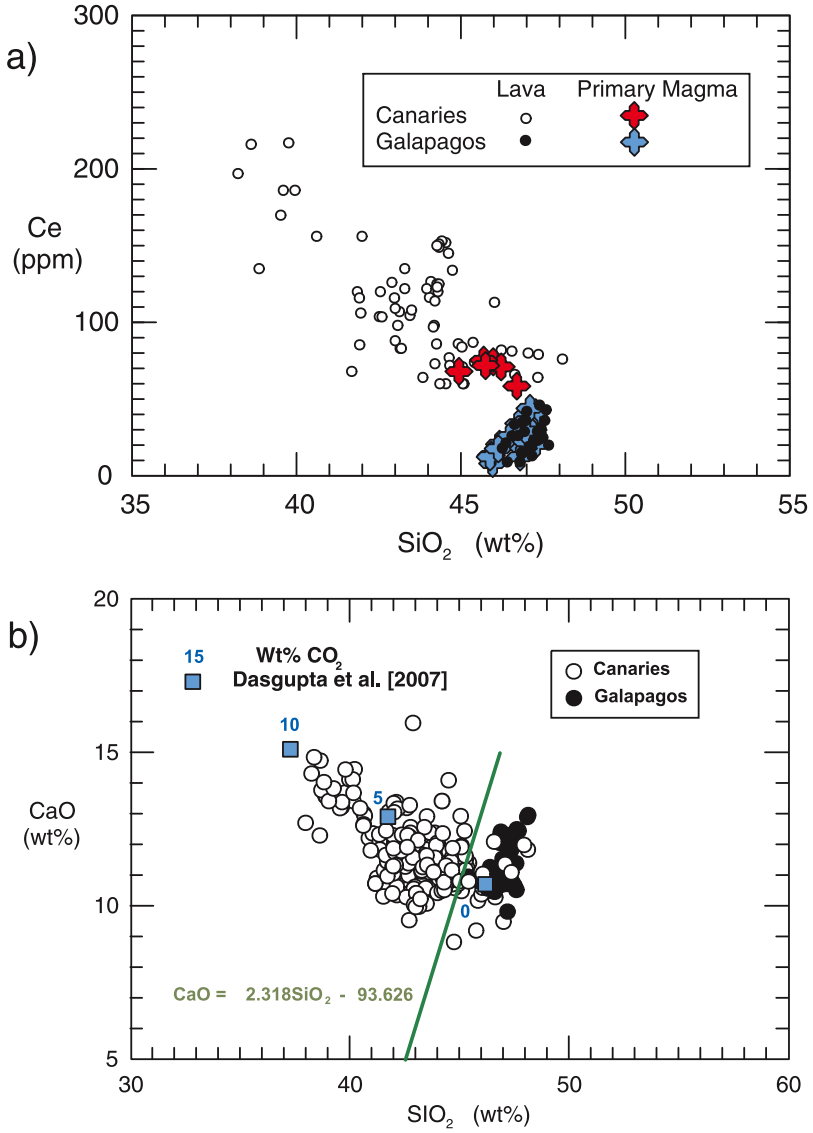

Figure 11. Contrasting geochemical properties of lavas from the Canary and Galápagos Islands. Only primitive lavas with MgO > 10% are shown in order to minimize the effects of Cpx fractionation in the crust. (a) SiO_2 and Ce contents of lavas and model primary magmas. Primary magmas have been estimated from lavas that plot to the right side of the green line in Figure 11b. (b) SiO_2 and CaO contents of lavas compared with partial melts of carbonated peridotite [*Dasgupta et al.*, 2007], modified from Figure 3. All primary magmas are derived from lavas that plot to the right side of the green line but are not shown for clarity. Primary magmas to the left cannot be derived with PRIMELT2 (see text).

recycled and melt to produce OIB, and that PRIMELT2 will identify such melt products if they reacted extensively with mantle peridotite.

[51] Many ocean islands reveal an important role played by melting recycled crust expressed lithologically as pyroxenite [*Sobolev et al.*, 2005, 2007; *Herzberg*, 2006], and this will contribute to source fertility. However, it is difficult to imagine how recycled crust can yield OIB sources with elevated $^3He/^4He$ [*Jackson et al.*, 2008]. We discussed in section 3 that lavas formed from pyroxenite and peridotite sources can often be distinguished using CaO, and our choice of peridotite-source OIBs is consistent with previous work [*Sun and McDonough*, 1989; *Jackson et al.*, 2008]. Application of the CaO filter together with the NiO tracer [*Sobolev et al.*, 2005] shows Mauna Kea melted from both peridotite and pyroxenite sources, both of which were equally hot (Figure 10) [*Herzberg*, 2006]. Similarly, the mantle sources below the ocean islands in the south Pacific have similar potential temperatures

(Figure 10), but different lithological characteristics. That is, the source for the Cook-Austral Islands is dominantly peridotite, whereas the sources for the Society Islands, Samoa, Pitcairn-Gambier and Marquesas are mixed peridotite and pyroxenite. There is no evidence that these ocean islands in the Pacific formed by melting recycled crust in the absence of a thermal anomaly.

[52] The range of mantle potential temperatures in Figure 10 may not be diagnostic of all oceanic islands on Earth. Many of these are highly differentiated lavas that have experienced substantial crystallization of olivine, plagioclase, and augite, and to these PRIMELT2 cannot be applied. When we have the ability to better constrain the problem for all cases, it is expected that some OIBs may not be associated with thermal anomalies. However, for the OIB cases examined in this paper, the range of T_P and the high thermal maxima shown in Figure 10 are diagnostic properties of their mantle sources. The only geodynamic model that displays such large variations is the mantle plume model wherein T_P increases from the periphery to the axis [*Ribe and Christensen*, 1999; *Farnetani and Samuel*, 2005].

12. Conclusions

[53] The PRIMELT2 algorithm and its realization in the PRIMELT2.XLS software is introduced for calculating primary magma compositions from observed lava compositions and the subsequent inference of mantle potential temperature. It supersedes PRIMELT1.XLS [*Herzberg et al.*, 2007] in that it has a wider range of applications and includes flags and filters that warn the user of a number of petrological complexities that compromise primary magma solutions and inferred potential temperatures. These are variations in source lithology, source volatile content, source oxidation state, and clinopyroxene fractionation, which can lead to overestimates in T_P by ~100°C. Collectively, the error can be even higher, leading to many ways to exaggerate the thermal properties of mantle sources. The most successful primary magma solutions are obtained for $Fe^{2+}/Fe^{Total} = 0.75–0.95$, extending to surprisingly low values for a number of ocean island suites, an inference that should be subject to further testing.

[54] Application of PRIMELT2.XLS to lavas from oceanic islands reveals sources that are hotter than ambient mantle, in agreement with previous studies [*Herzberg et al.*, 2007; *Courtier et al.*, 2007; *Putirka*, 2005; *Putirka et al.*, 2007]. There are also some important differences between PRIMELT2 temperature determinations and the others, but this paper is not intended to provide a critical review. PRIMELT2 calculates a range of potential temperatures and melt fractions for each OIB occurrence. For example, lavas from Mauna Kea on Hawaii record a T_P range of 1520–1600°C and a melt fraction range of 0.05–0.25 over a horizontal source distance of ~20 km. These results are consistent with the mantle plume model wherein T_P increases from the periphery to the axis [*Ribe and Christensen*, 1999; *Farnetani and Samuel*, 2005]. OIB T_P maxima are typically ~1450–1500°C in the Atlantic and 1500-1600°C in the Pacific, substantially greater than ~1350°C for ambient mantle. For the ocean islands considered in this work, there is no evidence that volatile-enrichment and source fertility are sufficient to produce them. All are associated with thermal anomalies, and this appears to be a prerequisite for their formation.

A1. Source and Lava Sample Identification for Successful Primary Magma Solutions

[55] All successful primary magma solutions were derived by the implementation of PRIMELT2.XLS on samples identified in Table A1. Lava compositions for these samples can be obtained either from the original sources listed in Table A1 or from GEOROC (http://georoc.mpch-mainz.gwdg.de/georoc/).

A2. Using PRIMELT2.XLS

[56] The primary magma calculations described in this paper are implemented in a publicly available Microsoft Excel workbook called PRIMELT2.XLS, which is provided as auxiliary material Software S1. Please note that this workbook uses Visual Basic for Applications (VBA) macros for several of the iterative calculations. As such, it is incompatible with Microsoft Office 2008 for Macintosh, which does not support VBA macros. There may be other incompatibility issues that we are not aware of, but it has been tested on Microsoft Windows XP 2002 using Microsoft Office 2004 and on MacOS 10.4 and 10.5 using Microsoft Office 2004. Upon opening the workbook you must choose to enable the macros or it will not function. Although PRIMELT1.XLS used iterated circular references, which required a particular

Table A1. Lava Sample Identification and Data Source for Primary Magma Calculation

Sample(s)	Source
Azores	
ASM36, SMB-6, SMB-7	*Widom et al.* [1997]
P26	*Turner et al.* [1997]
G-4, F-2	*White et al.* [1979]
2	*Canilho* [1970]
1, 10	*Rosenbaum* [1974]
SC4	*Renzullia and Santi* [2000]
Canary Islands	
A6 Leached, T1, T4	*Thirlwall et al.* [1997]
G1378, G1379	*Hoernle and Schmincke* [1993]
LP 134	*Marcantonio et al.* [1995]
12.861 ILM, 13.632 ILM	*Ibarrola* [1970]
16, 21	*Cendrero* [1966]
LPF96-46, LPF96-63	*Nikogosian et al.* [2002]
Cook-Austral Islands	
68D-2	*Stoffers et al.* [1989]
68DS-2	*Hémond et al.* [1994]
RPA-031 7263	*Dupuy et al.* [1988]
64-2, 68-2	*Hékinian et al.* [1991]
ATU114, ATU123	*Dupuy et al.* [1989]
RVV-139	*Barsczus and Liotard* [1985]
RRT-B-21, TBA-B-15	*Hauri and Hart* [1997]
2	*Wood* [1978]
RPA-488	*Lassiter et al.* [2003]
Galápagos Islands	
G86-3, FL-3, JH-86	*White et al.* [1993]
SC-23, SC-75	*Geist et al.* [1986]
JH-86	*Baitis and Swanson* [1976]
FL-3, FL-13, FL-30, FL-85, FL-25, FL-26, FL-78	*Bow and Geist* [1992]
SG93-19, SG93-22, SG93-23	*Kurz and Geist* [1999]
PL 13-12, PL 13-21	*Sinton et al.* [1993]
14, 50, 16, 42, 46, 47, 53, 54, 45A, Scoria	*Teasdale et al.* [2005]
Iceland	
408706, 408707, 408709, 408710, 408712	*Breddam* [2002]
Marquesas Islands	
6457, 6465	*Liotard et al.* [1986]
HTT-04, HTT-12, HGG-19	*Liotard and Barsczus* [1983]
70C	*Brousse* [1978]
Mauna Kea, Hawaii	
115-12, H-1	*Frey et al.* [1990]
MU-9, KI-8	*Frey et al.* [1991]
C-209	*Sobolev and Nikogosian* [1994]
C-71	*MacDonald and Katsura* [1964]
90/66110	*Muir and Tilley* [1963]
HQ-3, HU-7, IQ-15, JQ-13, JQ-17, JQ-25, JS-9, KI-8, MU-9	*Wolfe et al.* [1997]
SR0684-8.95, SR0684-9.00	*Stolper et al.* [2004]
Pitcairn-Gambier Islands	
80DS-2	*Woodhead and Devey* [1993]
FA682.7, MG5H	*Dupuy et al.* [1993]
709.1	*Guillou et al.* [1990]
G-AK-39	*Caroff et al.* [1993]
Samoan Islands	
131	*Stice* [1968]
63-3, 68-3, T16, T33, 76-9	*Workman et al.* [2004]
Society Islands	
TH-6, TH-8, TC-77	*Cheng et al.* [1993]
7-3	*Devey et al.* [1990]
8B	*Joron et al.* [1991]
81W1, 56Q, 81W, 56C	*Hildenbrand et al.* [2004]
St. Helena	
SH-7	*Barsikov et al.* [1979]
Tristan da Cunha	
64768	*Weaver et al.* [1987]

setting in the Calculation Preferences control panel, this is no longer needed with PRIMELT2.XLS.

[57] To use the program, we recommend creating a new worksheet by using the "Move or Copy Worksheet" operation, which can be accessed from the "Edit" menu as well as by a number of mouse and keyboard shortcuts that differ among operating systems. Name your new worksheet according to the sample name of the lava to be studied (by double-clicking on the title tab for this worksheet at the bottom of the window).

[58] Enter the oxide weight percent analysis of the sample in cells B4:N4 (yellow cells). Note that cell F4 asks for total Fe as FeO_T. The analysis need not be normalized; PRIMELT2.XLS will take care of this. Enter the desired Fe^{2+}/Fe_T as a mole fraction in cell F5. Alternatively, in order to use the method recommended in the text of adjusting Fe^{2+}/Fe_T in order to achieve a given Fe_2O_3/TiO_2 ratio, enter the desired Fe_2O_3/TiO_2 ratio in cell L5 and then click the nearby button labeled "Calculate Fe2+/Fe+", which will update the contents of cell F5 as needed. The only other user inputs are in cells R3:R4, where the FeO and MgO content of the source peridotite may be modified from the default values used in the calibration (KR4003), and in cell R6, where the pressure of the olivine fractionation/addition calculation can be changed (all the calculations in this paper use 1 bar; the program is only set up for isobaric fractionation/accumulation but the melting model is polybaric). Once information is input into these cells, the results appear in the output and warning cells automatically.

[59] If the input lava composition fails the peridotite/pyroxenite source test (section 3 above) or the volatile-rich peridotite source test (section 4 above), the text in cell G7 (orange fill) will change from "No Error" to a warning message, but the calculation will still proceed. If the accumulated fractional output primary magma composition fails either the clinopyroxene fractionation or accumulation test (section 5 above), an appropriate warning will appear at cell M13.

[60] Instantaneous fractional melts do not always mix to produce an accumulated fractional melt, an issue that was discussed by *Herzberg et al.* [2007]. These often have unusually low contents of FeO and high MgO, and they plot in the forbidden region below the curve labeled L + Ol in Figure 9a. The calculation will proceed anyway, but the user is alerted with the warning "FeO/MgO forbidden" in the orange-filled cell Q13. This warning will happen whenever the calculated primary magma content has an FeO content with the following characteristics:

$$\mathrm{FeO} < 0.577\mathrm{MgO} - 0.00026\mathrm{MgO}^3 + 5.48/\mathrm{MgO} \qquad \text{(A1)}$$

[61] Occasionally, a primitive lava rich in both MgO and Na_2O will display F3 < 0 in equation (6) even though SiO_2 is not unusually low. These are identified in PRIMELT2 as "negative normative quartz" in cells T9 or T13, and the primary magma solution is considered suspect.

[62] When the calculation is finished, the results appear in the green cells. The solution for batch melting appears in A11:W11 and the solution for accumulated fractional melting appears in cells A15:T15. In order from left to right, the meaning of the output cells is as follows:

[63] 1. %ol addition: The mass fraction of olivine added (or, if negative, subtracted) from the input lava composition to find the primary magma solution.

[64] 2. SiO2, TiO2...: The primary magma in oxide weight percent, including Fe_2O_3/FeO speciation. The MgO value is in boldface.

[65] 3. T: The "primary eruption temperature", as discussed by *Herzberg et al.* [2007]. It is the temperature at which the candidate primary magma occurs along the olivine control line at the specified fractionation pressure.

[66] 4. TP or TP_AFM: The mantle potential temperature calculated for the melting region to yield the appropriate primary magma; see *Herzberg et al.* [2007].

[67] 5. KD: The Fe/Mg distribution coefficient between olivine and the primary liquid composition, calculated at the primary eruption temperature and the fractionation pressure. See *Herzberg et al.* [2007] for the choice of KD models.

[68] 6. Xfo: The composition of the liquidus olivine that coexists with the primary liquid at the primary eruption temperature and fractionation pressure.

[69] 7. F (Fe/Mg) or F_AFM: equation (1) for batch melting; equation (3) for accumulated fractional melting.

[70] 8. Proj F1, F2, F3: equations (4), (5), and (6). Exactly one of these should equal F(Fe/Mg). If F(Fe/Mg) = F1, the solution is for a harzburgite or dunite residue; if F(Fe/Mg) = F2, the solution is for a spinel lherzolite residue, and if F(Fe/Mg) = F3, then the solution is for a garnet peridotite residue.

A3. Internal Consistency

[71] *Albarède et al.* [1997] concluded that clinopyroxene fractionation was important for understanding the geochemistry of lavas from Réunion and that this occurred at lithospheric mantle pressures. Indeed, this is indicated also by PRIMELT2 modeling. Of 66 high-MgO samples that have been modeled, PRIMELT2 warns that all but 3 of these have been compromised by clinopyroxene fractionation. And of the 3 successful primary magma solutions, 2 of these are suspect as shown in Figure A1. The 1 sample highlighted in green reveals a reasonable but not perfect level of internal consistency when viewed in MgO-FeO, MgO-SiO_2, and MgO-CaO space. By internal consistency, we refer to similar inferences drawn about pressures of initial (P_i) and final melting (P_f), and melt fraction (FAFM). For this sample, the following can be inferred: $P_i \cong$ 3.5 GPa, $P_f \cong$ 2.0–3.0 GPa, FAFM = 0.15–0.20. This level of consistency is not revealed, however, for any of the solutions colored red. Consider the solution having ~19.5% MgO. While similar melt fractions are inferred in MgO-FeO and MgO-SiO_2 (Figures A1a and A1b), $P_f \gg 3$ GPa in MgO-FeO, but only 2 GPa in MgO-CaO. The low value for P_f in MgO-CaO is mostly likely to be an artifact of Cpx fractionation, even though this is within the window of acceptability for PRIMELT2. For the solution having ~20.5% MgO, the melt fraction is 0.19 in MgO-FeO but ~0.27 in MgO-SiO_2.

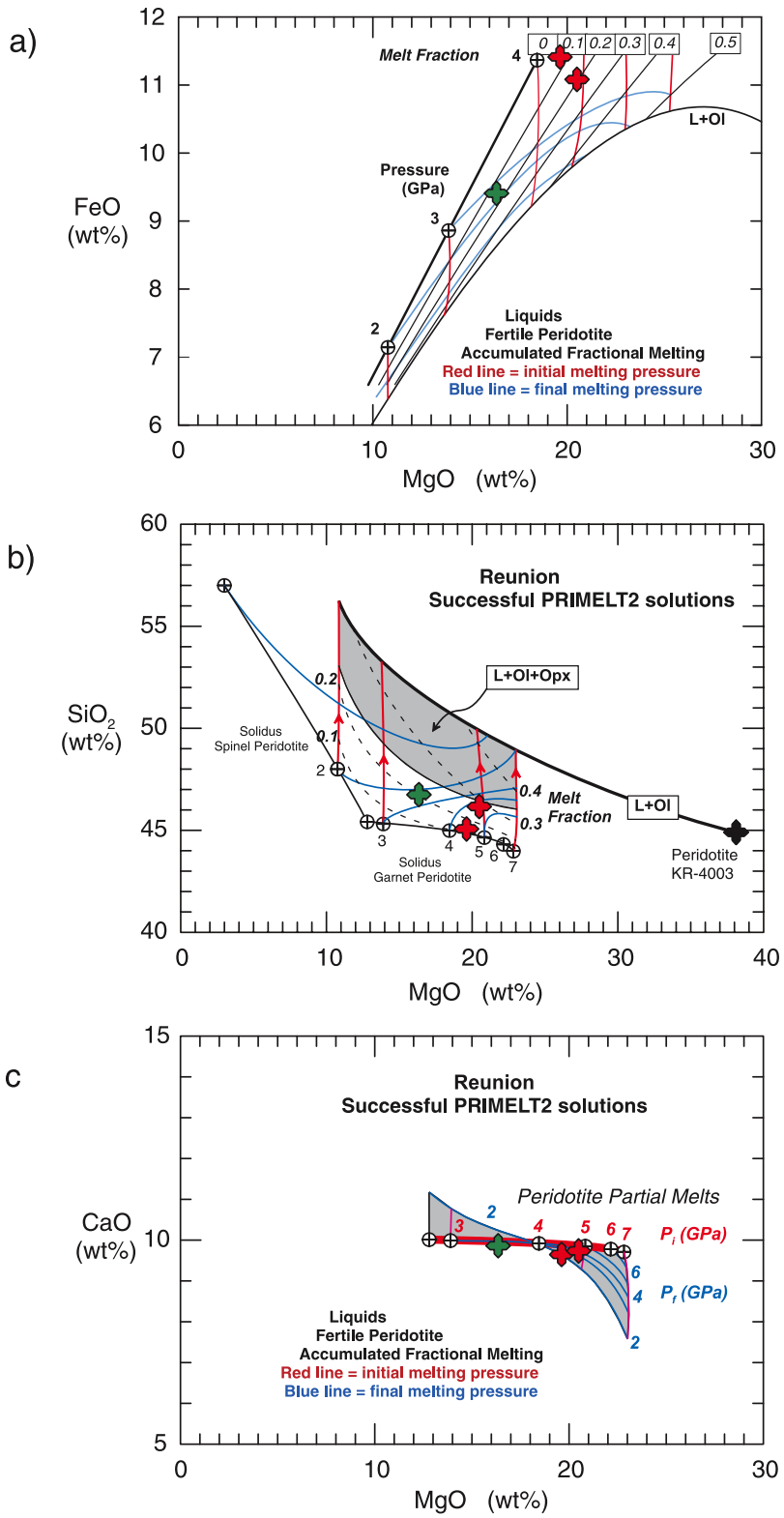

Figure A1. A graphical method for evaluating internal consistency for a primary magma solution. Successful PRIMELT2 solutions are shown for Réunion by the green and red symbols. However, only the green colored solution is internally consistent in the sense of revealing similar pressures of initial melting, final melting, and melt fraction in MgO-FeO, MgO-SiO_2, and MgO-CaO.

[72] We discussed in section 3 that high-CaO partial melts of pyroxenite can also yield primary magma solutions with poor internal consistency. Alteration of a lava can also compromise internal consistency. For example, palagonitization has been described in lavas from the Azores [*Furnes*, 1980], and this can lower CaO. The ability to recognize variable extents of alteration of a lava composition has been an outstanding problem in petrology and geochemistry, and PRIMELT2 has little to contribute to its resolution at the present time. However, a later version of this software will provide the required mathematical parameterization and description of pressures of initial and final melting (i.e., P_i, P_f) and melt fraction FAFM in MgO-SiO_2 and MgO-CaO. In the absence of this upgraded capability, the MgO-SiO_2 diagram can be obtained from Appendix 1 of *Herzberg* [2004]. And the MgO-CaO diagram showing P_i and P_f can be obtained from *Herzberg* [2006]; isopleths of melt fraction are highly compressed in this diagram, and are not shown. Internal consistency can be checked by plotting PRIMELT2 solutions on to these diagrams and reading P_i, P_f, and FAFM from them.

Acknowledgments

[73] Kaj Hoernle and Mike Rhodes are thanked for discussions. We are grateful to John Longhi and Cin-Ty Lee for thoughtful reviews. P.D.A. is supported by the NSF through grant OCE-0550216.

References

Albarède, F. (2008), Rogue mantle helium and neon, *Science*, *319*, 943–945, doi:10.1126/science.1150060.

Albarède, F., B. Luais, G. Fitton, M. Semet, E. Kaminski, B. G. J. Upton, P. Bachèlery, and J.-L. Cheminée (1997), The geochemical regimes of Piton de la Fournaise volcano (Réunion) during the last 530000 years, *J. Petrol.*, *38*, 171–201, doi:10.1093/petrology/38.2.171.

Anderson, D. L. (2000), The thermal state of the upper mantle: No role for mantle plumes, *Geophys. Res. Lett.*, *27*, 3623–3626, doi:10.1029/2000GL011533.

Anderson, D. L. (2007), The eclogite engine: Chemical geodynamics as a Galileo thermometer, in *Plates, Plumes and Planetary Processes*, edited by G. R. Foulger and D. M. Jurdy, *Spec. Pap. Geol. Soc. Am. Spec.*, *430*, 47–64, doi:10.1130/2007.2430(02).

Asimow, P. D., and J. Longhi (2004), The significance of multiple saturation points in the context of polybaric near-fractional melting, *J. Petrol.*, *45*, 2349–2367, doi:10.1093/petrology/egh043.

Asimow, P. D., M. M. Hirschmann, and E. M. Stolper (2001), Calculation of peridotite partial melting from thermodynamic models of minerals and melts, IV. Adiabatic decompression and the composition and mean properties of mid-ocean ridge basalts, *J. Petrol.*, *42*, 963–998, doi:10.1093/petrology/42.5.963.

Asimow, P. D., J. E. Dixon, and C. H. Langmuir (2004), A hydrous melting and fractionation model for mid-ocean ridge basalts: Application to the Mid-Atlantic Ridge near the Azores, *Geochem. Geophys. Geosyst.*, *5*, Q01E16, doi:10.1029/2003GC000568.

Baitis, H. W., and F. J. Swanson (1976), Ocean rise-like basalts within the Galápagos Archipelago, *Nature*, *259*, 195–197, doi:10.1038/259195a0.

Barsczus, H. G., and J.-M. Liotard (1985), Contribution to the petrography and geochemistry of Raivavae Island, French Polynesia, South-Central Pacific Ocean, *C. R. Acad. Sci, Ser. II*, *301*, 1409–1412.

Barsikov, V. L., L. N. Kogarko, A. I. Polyakov, K. I. Ignatenko, and A. I. Zinovev (1979), Differentiation of basaltoid melts and formation of the volcanic rock series of the South Atlantic islands, *Geochem. Int.*, *16*(6), 1–12.

Beattie, P. (1993), Olivine-melt and orthopyroxene-melt equilibria, *Contrib. Mineral. Petrol.*, *115*, 103–111, doi:10.1007/BF00712982.

Bonath, E. (1990), Not so hot "hot spots" in the oceanic mantle, *Science*, *250*, 107–111, doi:10.1126/science.250.4977.107.

Bow, C. S., and D. Geist (1992), Geology and petrology of Floreana Islands, Galápagos Archipelago, Ecuador, *J. Volcanol. Geotherm. Res.*, *52*, 83–105, doi:10.1016/0377-0273(92)90134-Y.

Breddam, K. (2002), Kistufell: Primitive melt from the Iceland mantle plume, *J. Petrol.*, *43*, 345–373, doi:10.1093/petrology/43.2.345.

Brousse, R. (1978), Analysis of several Marquesas Islands: Fatuhiva, Tahuata, Motane, Uapou, *Cah. Pac.*, *21*, 107–144.

Canilho, M. H. (1970), Possible origin of olivine nodules in basaltic lavas of Faial Azores, *Bol. Mus. Lab. Mineral. Geol. Fac. Cienc. Univ. Lisboa*, *11*, 193–198.

Carmichael, I. S. E. (1991), The redox states of basic and silicic magmas: A reflection of their source regions?, *Contrib. Mineral. Petrol.*, *106*, 129–141, doi:10.1007/BF00306429.

Caroff, M., R. C. Maury, G. Guille, H. Bellon, and J. Cotten (1993), Basalts of the Gambier Archipelago, French Polynesia, *C. R. Acad. Sci, Ser. II*, *317*, 359–366.

Carr, M. J., M. D. Feigenson, L. C. Patino, and J. A. Walker (2003), Volcanism and geochemistry in Central America: Progress and problems, in *Inside the Subduction Factory*, *Geophys. Monogr. Ser.*, vol. 138, edited by J. Eiler, pp. 153–179, AGU, Washington, D. C.

Cartigny, P., F. Pineau, C. Aubaud, and M. Javoy (2008), Towards a consistent mantle carbon flux estimate: Insights from volatile systematics (H_2O/Ce, δD, CO_2/Nb) in the North Atlantic mantle (14°N and 34°N), *Earth Planet. Sci. Lett.*, *265*, 672–685, doi:10.1016/j.epsl.2007.11.011.

Cendrero, U. A. (1966), The recent volcanoes of Fuerteventura (Canary Islands), *Estud. Geol.*, *22*, 201–226.

Cheng, Q. C., J. D. MacDougall, and G. W. Lugmair (1993), Geochemical studies of Tahiti, Teahitia and Mehetia, Society Island chain, *J. Volcanol. Geotherm. Res.*, *55*, 155–184, doi:10.1016/0377-0273(93)90096-A.

Courtier, A. M. (2007), Correlation of seismic and petrological thermometers suggests deep thermal anomalies beneath hotspots, *Earth Planet. Sci. Lett.*, *264*, 308–316, doi:10.1016/j.epsl.2007.10.003.

Dasgupta, R., M. M. Hirschmann, and N. D. Smith (2007), Partial melting experiments on peridotite+CO_2 at 3 GPa and genesis of alkalic ocean island basalts, *J. Petrol.*, *48*, 2093–2124, doi:10.1093/petrology/egm053.

Devey, C. W., F. Albarède, J.-L. Cheminée, A. Michard, R. K. Mühe, and P. Stoffers (1990), Active submarine volcanism on the Society hotspot swell (West Pacific): A geochemical study, *J. Geophys. Res.*, *95*, 5049–5066, doi:10.1029/JB095iB04p05049.

Dixon, J. E., L. Leist, C. Langmuir, and J.-G. Schilling (2002), Recycled dehydrated lithosphere observed in plume-influenced mid-ocean-ridge basalt, *Nature*, *420*, 385–389, doi:10.1038/nature01215.

Dupuy, C., H. G. Barsczus, J.-M. Liotard, and J. Dostal (1988), Trace element evidence for the origin of ocean island basalts: And example from the Austral Islands (French Polynesia), *Contrib. Mineral. Petrol.*, *98*, 293–302, doi:10.1007/BF00375180.

Dupuy, C., H. G. Barsczus, J. Dostal, P. Vidal, and J.-M. Liotard (1989), Subducted and recycled lithosphere as the mantle sources of ocean island basalts from Southern Polynesia, Central Pacific, *Chem. Geol.*, *77*, 1–18, doi:10.1016/0009-2541(89)90010-7.

Dupuy, C., P. Vidal, R. C. Maury, and G. Guille (1993), Basalts from Mururoa, Fangataufa, and Gambier Islands (French Polynesia): Geochemical dependence on the age of the lithosphere, *Earth Planet. Sci. Lett.*, *117*, 89–100, doi:10.1016/0012-821X(93)90119-T.

Eisele, J., W. Abouchami, S. J. G. Galer, and A. W. Hofmann (2003), The 320 kyr Pb isotope evolution of Mauna Kea lavas recorded in the HSDP-2 drill core, *Geochem. Geophys. Geosyst.*, *4*(5), 8710, doi:10.1029/2002GC000339.

Farnetani, C. G., and H. Samuel (2005), Beyond the thermal plume paradigm, *Geophys. Res. Lett.*, *32*, L07311, doi:10.1029/2005GL022360.

Frey, F. A. (1980), The origin of pyroxenites and garnet pyroxenites from Salt Lake Crater, Oahu, Hawaii: Trace element evidence, *Am. J. Sci.*, *280-A*, 427–449.

Frey, F. A., W. S. Wise, M. O. Garcia, H. B. West, S.-T. Kwon, and A. K. Kennedy (1990), Evolution of Mauna Kea volcano, Hawaii: Petrologic and geochemical constraints on postshield volcanism, *J. Geophys. Res.*, *95*, 1271–1300, doi:10.1029/JB095iB02p01271.

Frey, F. A., M. O. Garcia, W. S. Wise, A. K. Kennedy, P. Gurriet, and F. Albarède (1991), The evolution of Mauan Kea volcano, Hawaii: Petrogenesis of tholeiitic and alkalic basalts, *J. Geophys. Res.*, *96*, 14,347–14,375, doi:10.1029/91JB00940.

Furnes, H. (1980), Chemical changes during palagonitizatin of an alkaline olivine basaltic hyaloclastite, Santa Maria, Azores, *Neues Jahrb. Mineral Abh.*, *138*, 14–30.

Geist, D., A. R. McBirney, and R. A. Duncan (1986), Geology and petrogenesis of lavas from San Cristobal Island, Galápagos Archipelago, *Geol. Soc. Am. Bull.*, *97*, 555–566, doi:10.1130/0016-7606(1986)97<555:GAPOLF>2.0.CO;2.

Green, D. H., and T. J. Falloon (1998), Pyrolite: A Ringwood concept and its current expression, in *The Earth's Mantle: Composition, Structure, Evolution*, pp. edited by E. Jackson, 311–378, Cambridge Univ. Press, New York.

Guillou, H., G. Guille, R. Brousee, and J.-M. Bardintzeff (1990), Evolution of tholeiitic basalts and alkali basalts of Fangatuafa (French Polynesia), *Bull. Soc. Geol. Fr.*, *8*, 537–549.

Hauri, E., and S. R. Hart (1997), Rhenium abundances and systematics in oceanic basalts, *Chem. Geol.*, *139*, 185–205, doi:10.1016/S0009-2541(97)00035-1.

Hékinian, R., D. Bideau, P. Stoffers, J.-L. Cheminée, R. K. Mühe, D. Puteanus, and N. Binard (1991), Submarine intraplate volcanism in the South Pacific: Geological setting and petrology of the Society and the Austral regions, *J. Geophys. Res.*, *96*, 2109–2138, doi:10.1029/90JB02139.

Hémond, C., C. W. Devey, and C. Chauvel (1994), Source compositions and melting processes in the Society and Austral plumes (South Pacific Ocean): Element and isotope (Sr, Nd, Pb, Th) geochemistry, *Chem. Geol.*, *115*, 7–45, doi:10.1016/0009-2541(94)90143-0.

Herzberg, C. (2004), Geodynamic information in peridotite petrology, *J. Petrol.*, *45*, 2507–2530, doi:10.1093/petrology/egh039.

Herzberg, C. (2006), Petrology and thermal structure of the Hawaiian plume from Mauna Kea volcano, *Nature*, *444*, 605–609, doi:10.1038/nature05254.

Herzberg, C., and M. J. O'Hara (2002), Plume-associated ultramafic magmas of Phanerozoic age, *J. Petrol.*, *43*, 1857–1883, doi:10.1093/petrology/43.10.1857.

Herzberg, C., and J. Zhang (1996), Melting experiments on anhydrous peridotite KLB-1: Compositions of magmas in the upper mantle and transition zone, *J. Geophys. Res.*, *101*, 8271–8295, doi:10.1029/96JB00170.

Herzberg, C., P. D. Asimow, N. Arndt, Y. Niu, C. M. Lesher, J. G. Fitton, M. J. Cheadle, and A. D. Saunders (2007), Temperatures in ambient mantle and plumes: Constraints from basalts, picrites, and komatiites, *Geochem. Geophys. Geosyst.*, *8*, Q02006, doi:10.1029/2006GC001390.

Hildenbrand, A., P.-Y. Gillot, and I. Le Roy (2004), Volcano-tectonic and geochemical evolution of an oceanic intra-plate volcano: Tahiti-Nui (French Polynesia), *Earth Planet Sci. Lett.*, *217*, 349–365, doi:10.1016/S0012-821X(03)00599-5.

Hirschmann, M. M., T. Kogiso, M. B. Baker, and E. M. Stolper (2003), Alkalic magmas generated by partial melting of garnet pyroxenite, *Geology*, *31*, 481–484, doi:10.1130/0091-7613(2003)031<0481:AMGBPM>2.0.CO;2.

Hoernle, K. A. (1987), General geology and petrology of the Roque Nublo Volcanics on Gran Canarie, Canary Islands, Spain, M. A. thesis, Univ. of Calif., Santa Barbara, 191 pp., Santa Barbara.

Hoernle, K. A., and H.-U. Schmincke (1993), The petrology of the tholeiites through melilite nephelinites on Gran Canaria, Canary Islands: Crystal fractionation, accumulation, and depth of melting, *J. Petrol.*, *34*, 573–597.

Ibarrola, M. E. (1970), Variability of basaltic magmas in the eastern and central Canary Islands, *Estud. Geol.*, *26*, 337–399.

Irving, A. J. (1980), Petrology and geochemistry of composite ultramafic xenoliths in alkalic basalts and implications for magmatic processes within the mantle, *Am. J. Sci.*, *280-A*, 389–426.

Iwamori, H., D. McKenzie, and E. Takahashi (1995), Melt generation by isentropic mantle upwelling, *Earth Planet. Sci. Lett.*, *134*, 253–266, doi:10.1016/0012-821X(95)00122-S.

Jackson, M. G., S. R. Hart, A. E. Saal, N. Shimizu, M. D. Kurz, J. S. Blusztajn, and A. C. Skovgaard (2008), Globally elevated titanium, tantalum, and niobium (TITAN) in ocean island basalts with high $^{3}He/^{4}He$, *Geochem. Geophys. Geosyst.*, *9*, Q04027, doi:10.1029/2007GC001876.

Jakobsson, S., and J. R. Holloway (2008), Mantle melting in equilibrium with an iron-wüstite-graphite buffered COH-fluid, *Contrib. Mineral. Petrol.*, *155*, 247–256, doi:10.1007/s00410-007-0240-6.

Joron, J.-L., P. Schiano, L. Turpin, M. Treuil, T. Gisbert, C. Leotot, and R. Brousse (1991), Exceptional rare earth element enrichments in Tahaa volcano (French Polynesia), *C. R. Acad. Sci., Ser. II*, *313*, 523–530.

Kawamoto, T., and J. R. Holloway (1997), Melting temperature and partial melt chemistry of H2O-saturated mantle peridotite to 11 gigapascals, *Science*, *276*, 240–243, doi:10.1126/science.276.5310.240.

Kelemen, P. B., S. R. Hart, and S. Bernstein (1998), Silica enrichment in the continental upper mantle via melt/rock reaction, *Earth Planet. Sci. Lett.*, *164*, 387–406, doi:10.1016/S0012-821X(98)00233-7.

Keshav, S., G. H. Gudfinnsson, G. Sen, and Y.-W. Fei (2004), High-pressure melting experiments on garnet clinopyroxenite and the alkalic to tholeiitic transition in ocean-island basalts, *Earth Planet. Sci. Lett.*, *223*, 365–379, doi:10.1016/j.epsl.2004.04.029.

Keshav, S., G. Sen, and D. C. Presnall (2007), Garnet-bearing xenoliths from Salt Lake Crater, Oahu, Hawaii: High-pressure fractional crystallization in the oceanic mantle, *J. Petrol.*, *48*, 1681–1724, doi:10.1093/petrology/egm035.

Kogiso, T., and M. M. Hirschmann (2001), Experimental study of clinopyroxenite partial melting and the origin of ultracalcic melt inclusions, *Contrib. Mineral. Petrol.*, *142*, 347–360.

Kogiso, T., and M. M. Hirschmann (2006), Partial melting experiments of bimineralic eclogite and the role of recycled mafic oceanic crust in the genesis of ocean island basalts, *Earth Planet. Sci. Lett.*, *249*, 188–199, doi:10.1016/j.epsl.2006.07.016.

Kogiso, T., M. M. Hirschmann, and D. J. Frost (2003), High-pressure partial melting of garnet pyroxenite: Possible mafic lithologies in the source of ocean island basalts, *Earth Planet. Sci. Lett.*, *216*, 603–617, doi:10.1016/S0012-821X(03)00538-7.

Kurz, M. D., and D. Geist (1999), Dynamics of the Galápagos hotspot from helium isotope geochemistry, *Geochim. Cosmochim. Acta*, *63*, 4139–4156, doi:10.1016/S0016-7037(99)00314-2.

Langmuir, C. H., E. M. Klein, and T. Plank (1992), Petrological systematics of mid-ocean ridge basalts: Constraints on melt generation beneath ocean ridges, in *Mantle Flow and Melt Generation at Mid-Ocean Ridges*, *Geophys. Monogr. Ser*, vol. 71, edited by J. P. Morgan, D. K. Blackman, and J. M. Sinton, pp. 183–280, AGU, Washington, D. C.

Lassiter, J. C., J. Blichert-Toft, E. H. Hauri, and H. G. Barsczus (2003), Isotope and trace element variations in lavas from Raivavae and Rapa, Cook-Austral Islands: Constraints on the nature of HIMU- and EM-mantle and the origin of mid-plate volcanism in French Polynesia, *Chem. Geol.*, *202*, 115–138, doi:10.1016/j.chemgeo.2003.08.002.

Liotard, J.-M., and H. G. Barsczus (1983), Contribution to the petrography and geochemistry of Hatutu Island, Marquesas Archipelago, French Polynesia, South-Central Pacific Ocean, *C. R. Acad. Sci., Ser. II*, *297*, 725–728.

Liotard, J.-M., H. G. Barsczus, C. Dupuy, and J. Dostal (1986), Geochemistry and origin of basaltic lavas from Marquesas Archipelago, French Polynesia, *Contrib. Mineral. Petrol.*, *92*, 260–268, doi:10.1007/BF00375299.

Liu, Y., S. Gao, P. B. Kelemen, and W. Xu (2008), Recycled crust controls contrasting source compositions of Mesozoic and Cenozoic basalts in the North China Craton, *Earth Planet. Sci. Lett.*, *72*, 2349–2376.

Longhi, J. (1992), Origin of green glass magmas by polybaric fractional fusion, *Proc. Lunar Planet. Sci.*, *XXII*, 343–353.

Longhi, J. (2002), Some phase equilibrium systematics of lherzolite melting: I, *Geochem. Geophys. Geosyst.*, *3*(3), 1020, doi:10.1029/2001GC000204.

Longhi, J. (2006), Petrogenesis of picritic mare magmas: Constraints on the extent of early lunar differentiation, *Geochim. Cosmochim. Acta*, *70*, 5919–5934, doi:10.1016/j.gca.2006.09.023.

Longhi, J., and C. M. Bertka (1996), Graphical analysis of pigeonite-augite liquidus equilibria, *Am. Mineral.*, *81*, 685–695.

MacDonald, G. A., and T. Katsura (1964), Chemical composition of Hawaiian lavas, *J. Petrol.*, *5*, 82–133.

Marcantonio, F., A. Zindler, T. R. Elliott, and H. Staudigel (1995), Os isotope systematics of La Palma, Canary Islands: Evidence for recycled crust in the mantle source of HIMU ocean island, *Earth Planet. Sci. Lett.*, *133*, 397–410, doi:10.1016/0012-821X(95)00092-Q.

McKenzie, D., and M. J. Bickle (1988), The volume and composition of melt generated by extension of the lithosphere, *J. Petrol.*, *29*, 625–679.

McKenzie, D., A. Stracke, J. Blichert-Toft, F. Albarède, K. Grönvold, and R. K. O'Nions (2004), Source enrichment processes responsible for isotopic anomalies in ocean island basalts, *Geochim. Cosmochim. Acta*, *68*, 2699–2724, doi:10.1016/j.gca.2003.10.029.

Muir, I. D., and C. E. Tilley (1963), Contributions to the petrology of Hawaiian basalts, Part 2. The tholeiitic basalts of Mauna Loa and Kilauea, with chemical analyses by J. H. Scoon, *Am. J. Sci.*, *261*, 111–128.

Nikogosian, I. K., T. R. Elliott, and J. L. R. Touret (2002), Melt evolution beneath thick lithosphere: A magmatic inclusion study of La Palma, Canary Islands, *Chem. Geol.*, *183*, 169–193, doi:10.1016/S0009-2541(01)00387-4.

Niu, Y., and M. J. O'Hara (2003), Origin of ocean island basalts: A new perspective from petrology, geochemistry, and mineral physics considerations, *J. Geophys. Res.*, *108*(B4), 2209, doi:10.1029/2002JB002048.

O'Hara, M. J., and H. S. Yoder Jr. (1967), Formation and fractionation of basic magmas at high pressures, *Scot. J. Geol.*, *3*, 67–117.

Pilet, S., J. Hernandez, P. Sylvester, and M. Poujol (2005), The metasomatic alternative for ocean island basalt chemical heterogeneity, *Earth Planet. Sci. Lett.*, *236*, 148–166, doi:10.1016/j.epsl.2005.05.004.

Pilet, S., M. Baker, and E. M. Stolper (2008), Metasomatized lithosphere and the origin of alkaline lavas, *Science*, *320*, 916–919, doi:10.1126/science.1156563.

Putirka, K. D. (2005), Mantle potential temperatures at Hawaii, Iceland, and the mid-ocean ridge system, as inferred from olivine phenocrysts: Evidence for thermally driven mantle plumes, *Geochem. Geophys. Geosyst.*, *6*, Q05L08, doi:10.1029/2005GC000915.

Putirka, K. D., M. Perfit, F. J. Ryerson, and M. G. Jackson (2007), Ambient and excess mantle temperatures, olivine thermometry, and active vs. passive upwelling, *Chem. Geol.*, *241*, 177–206, doi:10.1016/j.chemgeo.2007.01.014.

Renzullia, A., and P. Santi (2000), Two-stage fractionation history of the alkali basalt-trachyte series of Sete Cidades volcano (Sao Miguel Island Azores), *Eur. J. Mineral.*, *12*, 469–494.

Rhodes, J. M., and M. J. Vollinger (2005), Ferric/ferrous ratios in 1984 Mauna Loa lavas: A contribution to understanding the oxidation state of Hawaiian magmas, *Contrib. Mineral. Petrol.*, *149*, 666–674, doi:10.1007/s00410-005-0662-y.

Ribe, N. M., and U. R. Christensen (1999), The dynamical origin of Hawaiian volcanism, *Earth Planet. Sci. Lett.*, *171*, 517–531, doi:10.1016/S0012-821X(99)00179-X.

Rosenbaum, M. S. (1974), Basaltic volcanism in South-East Terceira, Azores, *Geol. Mag.*, *111*, 409–420.

Saal, A., E. H. Hauri, C. H. Langmuir, and M. R. Perfit (2002), Vapour undersaturation in primitive mid-ocean-ridge basalt

and the volatile content of Earth's upper mantle, *Nature*, *419*, 451–455, doi:10.1038/nature01073.

Sen, G. (1988), Petrogenesis of spinel lherzolite and pyroxenite suite xenoliths from the Koolau shield, Oahu, Hawaii: Implications for petrology of the post-eruptive lithosphere beneath Oahu, *Contrib. Mineral. Petrol.*, *100*, 61–91, doi:10.1007/BF00399440.

Shaw, D. M. (1970), Trace element fractionation during anatexis, *Geochim. Cosmochim. Acta*, *34*, 237–243, doi:10.1016/0016-7037(70)90009-8.

Sinton, C. W., D. W. Christie, V. L. Coombs, R. L. Nielsen, and M. R. Fisk (1993), Near-primary melt inclusions in anorthite phenocrysts from the Galápagos platform, *Earth Planet. Sci. Lett.*, *119*, 527–537, doi:10.1016/0012-821X(93)90060-M.

Sobolev, A. V., and I. K. Nikogosian (1994), Petrology of long-lived mantle plume magmatism: Hawaii, Pacific, and Reunion Island, Indian Ocean, *Petrology*, *2*(2), 111–144.

Sobolev, A. V., A. W. Hofmann, S. V. Sobolev, and I. K. Nikogosian (2005), An olivine-free mantle source of Hawaiian shield basalts, *Nature*, *434*, 590–597, doi:10.1038/nature03411.

Sobolev, A. V., et al. (2007), The amount of recycled crust in sources of mantle-derived melts, *Science*, *316*, 412–417, doi:10.1126/science.1138113.

Stice, G. D. (1968), Petrography of the Manu'a islands, Samoa, *Contrib. Mineral. Petrol.*, *19*, 343–357, doi:10.1007/BF00389417.

Stoffers, P., R. Botz, J.-L. Cheminée, C. W. Devey, V. Froger, G. P. Glasby, M. Hartmann, D. Puteanus, and H. H. Richnow (1989), Geology of MacDonald seamount region, Austral Islands: Recent hotspot volcanism in the South Pacific, *Mar. Geophys. Res.*, *11*, 101–112, doi:10.1007/BF00285661.

Stolper, E., S. Sherman, M. Garcia, M. Baker, and C. Seaman (2004), Glass in the submarine section of the HSDP2 drill core, Hilo, Hawaii, *Geochem. Geophys. Geosyst.*, *5*, Q07G15, doi:10.1029/2003GC000553.

Sun, S. S., and W. F. McDonough (1989), Chemical and isotopic systematics of oceanic basalts: Implications for mantle composition and processes, in *Magmatism in the Ocean Basins*, edited by A. D. Saunders and M. J. Norry, *Geol. Soc. Spec. Publ.*, *42*, 313-345.

Teasdale, R., D. Geist, M. D. Kurz, and K. S. Harpp (2005), 1998 eruption of Volcano Cerro Azul, Galápagos Islands: 1. Syn-eruptive petrogenesis, *Bull. Volcanol.*, *67*, 170–185, doi:10.1007/s00445-004-0371-9.

Teng, F.-Z., N. Dauphas, and R. T. Helz (2008), Iron isotope fractionation during magmatic differentiation in Kilauea Iki lava lake, *Science*, *320*, 1620–1622, doi:10.1126/science.1157166.

Thirlwall, M. F., C. Jenkins, P. Z. Vroon, and D. P. Mattey (1997), Crustal interaction during construction of ocean islands: Pb-Sr-Nd-O isotope geochemistry of the shield basalts of Gran Canaria, Canary Islands, *Chem. Geol.*, *135*, 233–262, doi:10.1016/S0009-2541(96)00118-0.

Toplis, M. J. (2005), The thermodynamics of iron and magnesium partitioning between olivine and liquid: Criteria for assessing and predicting equilibrium in natural and experimental systems*Contrib. Mineral. Petrol.*, *149*, 22–39, doi:10.1007/s00410-004-0629-4.

Turner, S. P., C. J. Hawkesworth, N. W. Rogers, and P. King (1997), U-Th isotope disequilibria and ocean island basalt generation in the Azores, *Chem. Geol.*, *139*, 145–164, doi:10.1016/S0009-2541(97)00031-4.

Walter, M. J. (1998), Melting of garnet peridotite and the origin of komatiite and depleted lithosphere, *J. Petrol.*, *39*, 29–60, doi:10.1093/petrology/39.1.29.

Weaver, B. L., D. A. Wood, J. Tarney, and J.-L. Joron (1987), Geochemistry of ocean island basalts from the South Atlantic, Ascension, Bouvet, St. Helena, Gough and Tristan da Cuhnha, in *Alkaline Igneous Rocks*, edited by J. G. Fitton and B. G. J. Upton, pp. 253–267, Geol. Soc. London, London.

Weyer, S., and D. A. Ionov (2007), Partial melting and melt percolation in the mantle: The message from Fe isotopes, *Earth Planet. Sci. Lett.*, *259*, 119–133, doi:10.1016/j.epsl.2007.04.033.

White, W. M., M. D. Tapia, and J.-G. Schilling (1979), The petrology and geochemistry of the Azores Islands, *Contrib. Mineral. Petrol.*, *69*, 201–213, doi:10.1007/BF00372322.

White, W. M., A. R. McBirney, and R. A. Duncan (1993), Petrology and geochemistry of the Galápagos Islands: Portrait of a pathological mantle plume, *J. Geophys. Res.*, *98*, 19,533–19,563, doi:10.1029/93JB02018.

Widom, E., R. W. Carlson, J. B. Gill, and H.-U. Schmincke (1997), Th-Sr-Nd-Pb isotope and trace element evidence for the origin of the Sao Miguel, Azores: Enriched mantle source, *Chem. Geol.*, *140*, 49–68, doi:10.1016/S0009-2541(97)00041-7.

Wolfe, E. W., W. S. Wise, and G. B. Dalrymple (1997), The geology and petrology of Mauna Kea volcano, Hawaii—A study of postshield volcanism, *U. S. Geol. Surv. Prof. Pap.*, *1557*, 1–129.

Wood, C. P. (1978), Petrology of Atiu and Mangaia, Cook Islands (Note), *N. Z. J. Geol. Geophys.*, *21*, 767–771.

Woodhead, J. D., and C. W. Devey (1993), Geochemistry of the Pitcairn seamounts: 1. Source character and temporal trends, *Earth Planet. Sci. Lett.*, *116*, 81–99, doi:10.1016/0012-821X(93)90046-C.

Workman, R. K., S. R. Hart, M. Jackson, M. Regelous, K. A. Farley, J. Blusztajn, M. Kurz, and H. Staudigel (2004), Recycled metasomatized lithosphere as the origin of the Enriched Mantle II (EM2) end-member: Evidence from the Samoan Volcanic Chain, *Geochem. Geophys. Geosyst.*, *5*, Q04008, doi:10.1029/2003GC000623.

Wright, T., D. A. Swanson, and W. A. Duffield (1975), Chemical compositions of Kilauea east-rift lava, 1968–1971, *J. Petrol.*, *16*, 110–133.